Environmental and Experimental Botany 241 (2026) 106281

Contents lists available at ScienceDirect

Environmental and Experimental Botany

journal homepage: www.elsevier.com/locate/envexpbot

Research Paper

Hydrochar from garden waste enhances drought tolerance in sunflower via soil-plant-gene interactions

Stefano Mileto [a], Damiano Spagnuolo [a], Antonio Lupini [b], Giovanna Battipaglia [c], Viviana Bressi [d], Claudia Espro [d], Giuseppa Genovese [a], Alessandro Crisafulli [a], Domenico Viglianti [b], Lucio Zaccariello [c], Patrizia Trifilò [a,*]

[a] Department of Chemical, Biological,Pharmaceutical and Environmental Sciences, University of Messina, Italy
[b] Department of Agraria, University Mediterranea of Reggio Calabria, Italy
[c] Department Environmental, Biological and Pharmaceutical Sciences and Technologies, University of Campania Luigi Vanvitelli, Italy
[d] Department of Engineering, University of Messina, Italy

ARTICLE INFO

Keywords:
Drought resilience
Hydrochar
RNA sequencing
Soil water retention
Transcriptomic profiling
Water use efficiency

ABSTRACT

Enhancing crop drought resilience is essential for sustainable agriculture in a changing climate. Among potential strategies, hydrochar (HC), a carbon-rich product of hydrothermal carbonization, represents a promising soil amendment. We hypothesized that HC enhances drought tolerance in *Helianthus annuus* L. through coordinated soil–plant–gene interactions that modulate water retention, plant hydraulics, and drought-responsive gene networks. Using a multiscale approach combining soil physicochemical analyses, plant physiology, and transcriptomics, we assessed the effects of garden waste-derived HC on *H. annuus* under well-watered and water-limited conditions. HC application improved soil water retention without altering key chemical parameters and enhanced plant hydraulics. Across irrigation regimes, HC-treated plants showed greater biomass accumulation and photosynthetic capacity. During drought, HC mitigated stress by maintaining leaf water potential and membrane integrity, and by promoting a more negative turgor loss point via osmotic adjustment and increased cell wall stiffness. Transcriptomic analysis revealed that HC modulated drought-responsive genes, including transcription factors (e.g., WRKY51, bZIP11) and genes involved in osmotic regulation, antioxidant defense, and hormonal signaling. The distinct molecular signature in HC-treated plants under drought suggests a priming effect that sustains physiological function under stress. This study provides novel evidence linking HC-induced soil enhancement to molecular drought responses in crops, highlighting HC's potential as a circular input for improving adaptation and productivity in climate-resilient agroecosystems.

1. Introduction

Climate change is accelerating vegetation decline and widespread plant mortality across natural ecosystems, with serious consequences for biodiversity and ecosystem functioning (Allen et al., 2015; Hammond et al., 2022). These impacts extend to managed landscapes, where agricultural systems face increasing exposure to more frequent and severe drought events, resulting in substantial yield losses in major crops (Iizumi et al., 2014; Lesk et al., 2022; Zhu et al., 2022). As global food demand continues to rise amid growing climatic instability, improving crop performance under water-limited conditions has become an urgent global priority (Molotoks et al., 2021; Kompas et al., 2024).

Projections indicate that growing season temperatures will rise faster than annual means, while precipitation is expected to decline, especially in vulnerable regions such as southern Europe and the Mediterranean basin (IPCC, 2022). These trends pose a major threat to plant physiological function and the stability of agroecosystems. Addressing this challenge requires integrated strategies that link plant physiology, molecular biology, and soil science within the framework of sustainable resource use.

Promising strategies to enhance drought resilience include soil amendments that improve water dynamics in the rhizosphere. Circular economy approaches, in this context, provide innovative pathways by converting organic waste into agronomically beneficial products. One such product is hydrochar (HC), a carbon-rich material obtained through hydrothermal carbonization (HTC), a thermochemical process

* Corresponding author.
E-mail address: ptrifilo@unime.it (P. Trifilò).

https://doi.org/10.1016/j.envexpbot.2025.106281
Received 10 July 2025; Received in revised form 12 October 2025; Accepted 24 November 2025
Available online 25 November 2025

that converts wet biomass into a stable, energy-dense solid (Reza et al., 2014). While initially developed for energy applications, HC is now gaining attention as a sustainable soil amendment due to its ability to improve water retention, nutrient availability, and microbial activity (Battipaglia et al., 2023; Kravchenko et al., 2024; Dong et al., 2025; Di Santo et al., 2025). Compared to traditional amendments such as compost or biochar, HC presents unique properties: a chemically uniform composition, rapid nutrient release, and the potential to stimulate biological activity, though with lower long-term stability (Kamb and Dutta, 2015; Yan et al., 2024). Its slightly acidic pH also makes it suitable for alkaline soils, where other amendments may be less effective (de Jager and Gianim, 2021).

Emerging evidence suggests that HC may influence plant regulatory pathways associated with stress response and nutrients release (Bargmann et al., 2014; Bento et al., 2019; Battipaglia et al., 2023; Suarez et al., 2025). However, the underlying mechanisms remain poorly understood, partly due to the variability in HC properties depending on feedstock type and processing conditions. Notably, HC derived from lignocellulosic green waste tends to exhibit enhanced nutrient content, lower contaminant levels, and greater agronomic potential compared to sludge-based materials (Taskin et al., 2019; Carrasco et al., 2022).

In this study, we adopt a multiscale, multidisciplinary approach to investigate the role of HC in modulating plant responses to water availability. Using *Helianthus annuus* L., an agronomically important species, we integrated soil physicochemical analyses, plant physiological measurements, and transcriptomic profiling (RNA-seq) under both well-watered and mild drought conditions.

By linking functional plant traits with gene expression and the chemical properties of soil, our study aims to provide mechanistic insights into how HC shapes plant performance under stress. This integrative framework advances our understanding of HC as a bio-based amendment and informs the development of next-generation strategies for climate-resilient agriculture.

2. Materials and methods

Experiments were conducted during the spring and summer of 2024. Sunflower seeds (*Helianthus annuus L. Girasole Nano Big Smile*, P.d.F. Sementi, Italy) were sown in greenhouse trays. Once the cotyledons had fully expanded (about 7 days after emergence of radicle), seedlings were transplanted into 2.5 L pots containing either commercial potting substrate (C samples) or the same substrate mixed with hydrochar (HC samples). The growth medium used in this study was a nutrient-rich substrate specifically formulated for vegetable growth, eliminating the need for additional fertilization (Comodo, Tercomposti S.P.A., Italy). Hydrochar, derived from the hydrothermal carbonization (HTC) of garden waste, was incorporated into the soil at a concentration of 22 g Kg^{-1}. This concentration was selected based on the findings of Battipaglia et al. (2023). The used hydrochar was obtained by setting the reactor at 230 °C for 4 h at a pressure of 5.0 MPa (for details, see Supplementary material).

Once the plants displayed fully expanded leaves (approximately 3 weeks old), C and HC plants follows:

- Control samples (Cw) and hydrochar-treated samples (HCw), to be regularly irrigated at field capacity during the experimental period.
- Control samples (C_D) and hydrochar-treated samples (HC_D) to be subjected to mild drought by suspending irrigation until the soil water potential (Ψ_{soil}) reached approximately −0.5 MPa, followed by irrigation to 100 % of field capacity and subjected to the same drought intensity once again (Supplementary Figure 1). The drought/re-irrigation treatment lasted for one month (Supplementary Figure 1).

All plants (Cw, HCw, C_D, HC_D) were grown in a greenhouse at the Department CHIBIOFARAM of the University of Messina, equipped with lamps providing photosynthetically active radiation (PAR) of 450 ± 30 μmol m^{-2} s^{-1}. Pots (n = 15 per treatment) were arranged in a completely randomized design in the greenhouse. Pots were weighed daily, and irrigation was applied based on their weight. The reference weight at 100 % corresponded to field capacity, determined after soil saturation and free drainage. Well-watered pots were kept between 100 % and ~90 % of this weight. In drought treatments, irrigation was suspended until soil water potential (Ψ_{soil}) reached −0.5 MPa, corresponding to ~75 % of field capacity in control soils and ~65 % in hydrochar-amended soils. These soil water potentials led sunflower plants to reach the turgor loss point (see Results). Thresholds were derived from the soil water retention curve (Fig. 1) and validated in measurements using a dewpoint hygrometer (WP4, Decagon Devices Inc., USA) readings on three sacrificed pots per treatment.

2.1. Evaluating physical-chemical traits of hydrochar

In order to obtain a detailed and comprehensive characterization of hydrochar, the following chemical and physical analyses were performed:

2.1.1. ***Fourier transfor infrared spectroscopy***

Fourier infrared spectra were acquired using a Fourier-Transform Infrared (FTIR) Spectrum Two FTIR Spectrometer 100 (PerkinElmer Inc.), which was equipped with a universal ATR sampling accessory. The spectra were recorded at room temperature within the range from 4000 to 500 cm^{-1}, with a scan speed of 0.2 cm/s, a resolution of 4.0 cm^{-1}, performing the analysis at room temperature and an accumulation scan of 50. The samples were analysed without any preliminary treatment.

2.1.2. *CHNS-O elemental analysis*

Elemental analysis of the sample was conducted using the EMA 502 Micro Elemental Analyzer CHNS-O (VELP® Scientifica). Before the analysis, hydrochar was dried overnight in an oven at 90°C to remove any residual moisture. The results were computed using the EMASoftTM software.

2.1.3. *Raman spectroscopy analysis*

Raman spectroscopy was carried out directly on the sample using a Horiba Labram HR800 confocal spectrometer (Horiba Jobin Yvon), equipped with a diode-pumped solid-state (DPSS) laser operating at an excitation wavelength of $\lambda_{ex} = 638$ nm.

2.1.4. *UV-Vis spectroscopy analysis*

Optical properties (UV–vis absorption) of hydrochar were studied using a spectrophotometer Evolution 500, Thermo Nicolet model (Thermo Fisher Scientific, Waltham, MA, USA) equipped with glass cuvettes (1 cm path length). All the recorded data were generated using OriginPro2019 software.

2.1.5. *Scanning electron microscopy (SEM)*

The morphology of hydrochar sample was investigated by using a Zeiss 1540XB FE SEM (Zeiss, Germany) instrument operating at 10 kV.

2.1.6. *X-ray diffraction (XRD) analysis*

The crystalline structure of the synthesized carbon material was examined through XRD analysis, performed using a Bruker D8 Advance A25 diffractometer. The instrument operated at 40 kV, scanning over a 2θ range of 10–80° with a step size of 0.02° s^{-1} , employing CuKα₁ radiation as the X-ray source.

2.1.7. *Thermogravimetric analysis (TGA)*

The thermal stability under an inert atmosphere was evaluated by TGA using a PerkinElmer TGA 4000, over a temperature range from 50 °C to 500 °C.

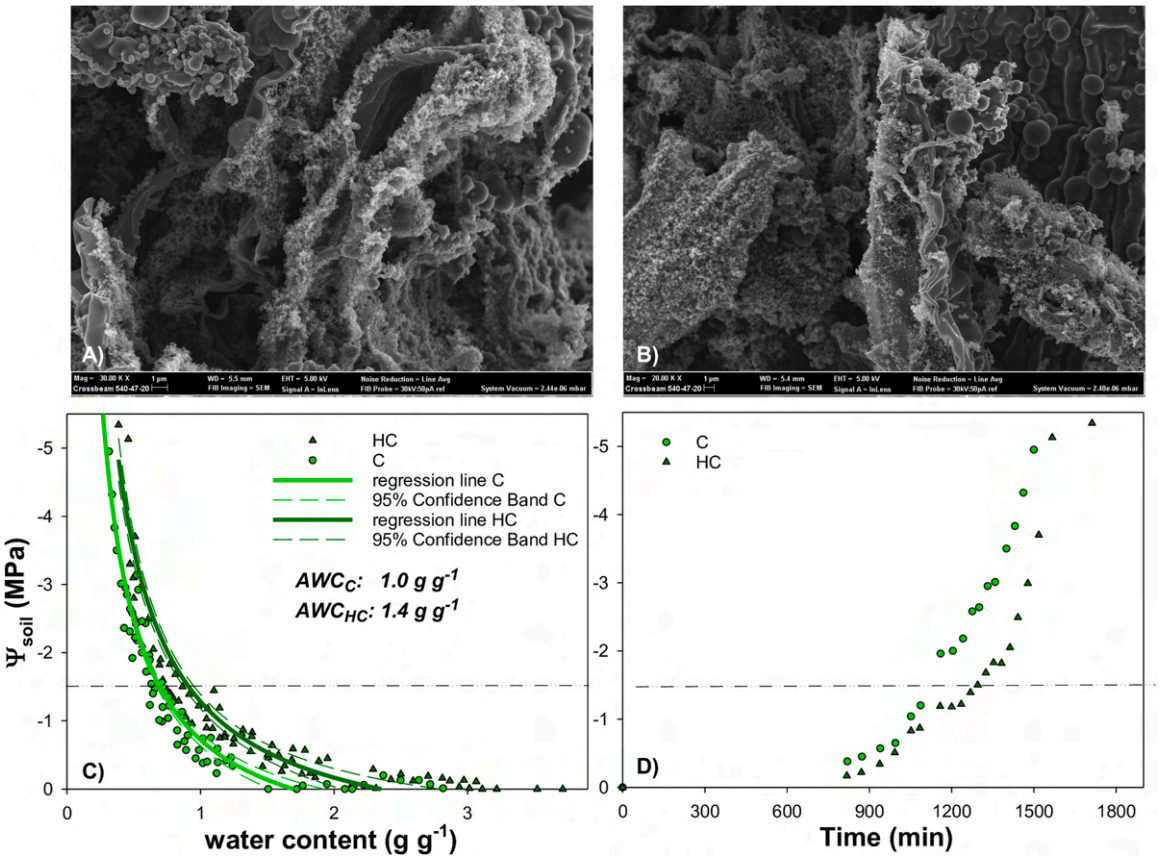

Fig. 1. A) and B) SEM images of hydrochar obtained from the hydrothermal process of garden waste; C) Moisture release curves, obtained by plotting the soil water potential (Ψ_{soil}) versus water content, as measured for samples of soil without hydrochar (C, green light circles) or soil with hydrochar (HC, dark green triangles). Available water content (AWC) was calculated from the regression line as the difference between field capacity and the permanent wilting point (-1.5 MPa, dotted line). D) Time of dehydration (Time) of two samples of soil (C, light green circles) and soil with hydrochar (HC, dark green triangles). The dotted line indicates the standard permanent wilting point of −1.5 MPa.

2.2. Water retention and chemical-physical properties of growing medium

To assess the impact of hydrochar addition on the chemical and physical properties of the soil, including its water retention capacity, several key parameters were measured.

Following USDA guidelines (2004), soil pH and electrical conductivity (EC) were determined using a calibrated electrode system (Hanna Instruments Mod. HI1230 and COND 51 +, respectively). Measurements were performed on aqueous suspensions of dry soil at soil-to-water ratios of 1:2.5 for pH and 1:2 for EC. The cation exchange capacity (CEC) was evaluated after soil treatment with a barium chloride and triethanolamine solution at pH 8.2 (USDA, 2004). Total organic carbon (Corg) content was determined using the Springer and Klee (1954) method, which involves oxidation in an acidic medium (H_2SO_4) with potassium dichromate (0.33 M $K_2Cr_2O_7$) under controlled heating (160°C for 10 min) to ensure complete recovery of organic carbon (Sleutel et al., 2007). These measurements were performed at the end of the experimental period on samples of the growing medium from pots containing Cw, HCw, C_D, and HC_D plants, as well as on soil samples from pots in which no plants were grown, collected before starting experiments.

To evaluate the water retention properties of the two growing medium used to grow *Helianthus annuus* L., commercial potting substrate alone (C) and the same substrate mixed with 6 Kg m^{-2} of hydrochar (HC), the relationship between soil water content (WC) and water potential (Ψ) during progressive dehydration was assessed (Raimondo et al., 2015). Specifically, substrate samples were saturated with water and, after draining the excess, small portions (a few grams) were placed in sample holders. Water potential was measured at different dehydration times using a dewpoint hygrometer (WP4, Decagon Devices Inc., USA). Immediately after each measurement, samples were weighed to determine their fresh weight (FW). Experiments were stopped at $\Psi \leq -5$ MPa, and samples were oven-dried at 70 °C for 24 h to obtain dry weight (DW). Water content (WC) was calculated as (FW − DW) /DW. The gravimetric available water content (AWC) values were calculated as the difference between the water content at saturation after free drainage (effectively corresponding to field capacity) and the water content of soil at the standard permanent wilting point of −1.5 MPa (Nardini et al., 2021).

2.3. Biomass and morpho-anatomical traits

The number of leaves and plant height were recorded weekly in five plants per treatment. At the end of the experimental period, these plants were used to measure biomass and morpho-anatomical traits. The total leaf surface area (A_L) was measured by capturing leaf images with a scanner (HP Scanjet G4050, USA) and using ImageJ software (http://imagej.nih.gov/ij/). Leaf mass per area (LMA) was estimated as DW/A_L and was calculated using the average LMA of three randomly collected leaves from each of the five plants per treatment. Additionally, plants were separated into roots (after gently rinsing to remove soil), stems, leaves, and buds/flowers, and the fresh mass of each organ was recorded. Stem diameter was measured using a digital caliper. The plant material was then dried in an oven at 80°C for 72 h to determine the dry weight (DW).

2.4. Pressure-volume curves

Leaf water potential isotherms (or pressure-volume, PV curves) were measured on 5 leaves per treatment to estimate: leaf water potential at the turgor loss point (Ψ_{tlp}), osmotic potential at full turgor (π_0), bulk modulus of elasticity (ε), leaf capacitance at full turgor (C_{ft}) and after the turgor loss point (C_{tlp}). PV curves were performed in a preliminary experiment on well-watered samples (Cw and HCw) to determine the established threshold value needed to induce drought. Additionally, PV curves were performed at the end of the experimental period to assess any possible changes in PV traits. To perform PV curves, leaves were cut under water and allowed to rehydrate for at least 1 h. Leaf water potential (Ψ_L) and leaf water loss were measured at regular intervals during progressive dehydration (Tyree and Hammel, 1972). Ψ_{tlp} was estimated as the flex point of the relationship between $1/\Psi_L$ and water loss. Moreover, π_0 was calculated by the y-intercept of the linear region of this relationship, and ε was calculated as $\Delta Pt/(\Delta W/W)$, where ΔPt is the change of turgor pressure and $\Delta W/W$ is the relative change of the leaf water content. Leaf capacitance was also derived from PV curves. Specifically, C_{ft} was estimated as: Δ(100-RWC)/($\Delta\Psi_L$ before Ψ_{tlp}) and C_{tlp} was estimated as: Δ(100-RWC)/($\Delta\Psi_L$ past Ψ_{tlp}), where RWC is the relative water content. The samples were finally dried in an oven for 3 days at 80 °C to obtain their DW. Additionally, the leaf-area specific C_{ft} (C^*_{ft}) and leaf-area specific C_{tlp} (C^*_{tlp}) were also estimated as: C^*_{ft}: C_{ft} x SWC x LMA; C^*_{tlp}= C_{tlp} x SWC x LMA x RWC_{tlp} where SWC is the saturated water content and RWC_{tlp} is the RWC at the turgor loss point.

2.5. Gas exchange, photosynthesis and plant hydraulic conductance measurements

Stomatal conductance to water vapor (g_L), transpiration rate (E_L), photosynthesis rate (An) (measured using a portable LCi Analyzer System, ADC Bioscientific Ltd., Herts) were measured starting three weeks after transferring the plants into pots. Measurements were performed diurnally at 11:00 am, five hours after the lamps were switched on. Additionally, leaf water potential (Ψ_L) was measured on the day drought treatment began (day 0), as well as two days after rewatering following the second (day 17) and third (day 27) drought cycles (Supplementary Figure 1). Ψ_L was measured on five leaves per treatment using a pressure bomb on the same leaves where E_L was recorded. Plant hydraulic conductance (K_{plant}) was then estimated using the formula: E_L / (Ψ_L - Ψ_{soil}), where Ψ_{soil} is the soil water potential measured by a dewpoint hygrometer (Model WP4, Decagon Devices Inc.) (Raimondo et al., 2015).

2.6. Relative electrolyte leakage

Leaf, stem and root electrolyte leakage measurements as proxy of cell membrane damage were measured at the end of the experimental period (Trifilò et al., 2023).

Leaf samples of about 1 cm^2, 2-cm long stem segments and root samples were cut with a razor blade and placed in test tubes containing 8 ml of distilled water. Tubes were then stirred for 30 min and the initial electrical conductivity of the solution (ECi) was recorded by a conductivity metre (Cond 5, XS instruments). Samples were then subjected to three freeze/thaw cycles (i.e., T = −20°C, +20°C) to induce membrane disruption and processed as above to estimate the final electrical conductivity of the solution (ECf). The relative electrolyte leakage, REL, was calculated as: (ECi/ECf) × 100.

2.7. Water use efficiency estimation (WUEi)

Intrinsic plant water use efficiency was determined through carbon stable isotopes analysis at the end of treatment. Stem, roots, leaves of the individuals *H. annuus* were air dried, pulverized with a pulverizing mill (ZM 1000, Retsch, Haan, Germany) and weighed in tin capsules for carbon isotopic measurements. The isotopic composition was measured at the IRMS laboratory of the University of Campania "Luigi Vanvitelli" by mass spectrometry with a continuous flow isotope ratio (Delta V Advantage, Thermo Scientific, Waltham, MA, USA). The standard deviation for the repeated analysis of an internal standard was better than 0.1 ‰. $\delta^{13}C$ data were used for computing the intrinsic water use efficiency (WUEi), a ratio between the carbon assimilation rate and stomatal conductance, following Farquhar's theoretical framework (Farquhar et al., 1982) which can be summarized by the equations 1 and 2.

$$\delta^{13}Cplant = \delta^{13}Catm - a - \frac{(b-a)ci}{ca}$$

$$WUEi = \frac{ca - ci}{1.6} = \frac{An}{gs}$$

Where a is the fractionation factor due to diffusion through the stomata (-4.4 ‰) and b is the fractionation factor of RUBISCO (-27 ‰). $\delta^{13}Catm$ and ca are the isotopic value of atmospheric CO_2 and its concentration, which are known, as well as the $\delta^{13}Cplant$ which is measured through the stable isotope measurements, ca is the CO_2 concentration in the atmosphere, while ci is the concentration of CO_2 in the intercellular spaces of the leaves, and 1.6 is the ratio of the diffusivity of water and CO_2 through the stomata, An is the net assimilation rate and gs is stomatal conductance. The gradient between the concentration of CO_2 inside the leave and outside is a direct result of the balance between photosynthesis, that subtracts CO_2 and stomatal conductance, which allows CO_2 to enter the leaf.

2.8. Transcriptomic analysis

For RNA-Seq analysis, sunflower leaf samples were collected on day 27 from the start of drought treatment and stored at −80 °C to ensure RNA integrity. To obtain a representative RNA expression profile three biological replications were used. Total RNA was extracted using the RNeasy mini kit (Qiagen, Hilden, North Rhine-Westphalia, Germany) according to the manufacturer's instructions. Quality and quantity of the isolated RNA were checked using a NanoDrop 1000 spectrophotometer (Thermo Scientific, Wilmington, Delaware, USA) and denaturing agarose gel electrophoresis. Finally, DNA was eliminated by treatment with TURBO DNA-free™ Kit (Thermo-Fisher).

2.9. RNA sequencing and data processing

Total RNA was used for sequencing libraries using Illumina Stranded mRNA Prep (Illumina Inc.). The library products were sequenced on the Illumina NovaSeq X plus platform, and 150 bp paired-end reads were generated. Raw read quality was checked using 'FastQC' (Andrews, 2010) and data were cleaned using Trim Galore (v. 3.0) (Krueger, 2021). After, the clean reads were mapped with STAR software (Dobin et al., 2013) into the sunflower reference genome HanXRQr2.0-SUNRISE (Badouin et al., 2017). Mapped reads were assigned to genes and quantified with 'featureCounts' (Liao et al., 2014). Downstream data analysis, as differential expresses genes (DEGs) was performed in R v. 4.1.2 (R Core Team, 2022) on data normalized using DESeq2 package (Love et al., 2014).

2.10. Gene ontology and KEGG enrichment

In order to evaluate gene ontology (GO) as well as KEGG pathway, the candidate DEGs were submitted to Database for Annotation, Visualization and Integrated Discovery (DAVID) (Sherman et al., 2022; Huang et al., 2009) by using sunflower reference genome (HanXRQr2.0-SUNRISE) as background. In addition, the three categories (biological process, BP; cellular component, CC; and molecular

Table 1
Means ± SD of: a) biomass traits, b) PV-derived traits, and c) intrinsic water use efficiency (WUEi) and d) relative electrolyte leakage (REL) recorded in well-watered (Cw and HCw) and drought-stressed (C_D and HC_D) *Helianthus annuus* plants. Different letters indicate statistically significant differences. Statistically significant differences were determined by two-way ANOVA, followed by Holm–Sidak post hoc tests, and are reported for the two growing media (GM: substrate, C; and substrate mixed with hydrochar, HC) and irrigation treatments (I: well-watered and drought-stressed). ns: not statistically significant; *: $P < 0.05$; **: $P < 0.01$; ***: $P < 0.001$. Hplant: plant height; LMA: leaf mass per area; DW: dry weight; Ψ_{tlp}: leaf water potential at the turgor loss point, $\pi_{0:}$ osmotic potential at full turgor, ε: bulk modulus of elasticity, RWC_{tlp}: relative water content at turgor loss point, C^*_{ft} and C^*_{tlp}: leaf-area specific capacitance at full turgor and after the turgor loss point, respectively.

	Cw	HCw	C_D	HC_D	GM	I	GM**I
a) Biomass	**traits** (n = 5)						
H plant (cm)	11.2 ± 1.4	14.6 ± 1.0	9.2 ± 2.0	11.6 ± 2.4	**	*	ns
Ø (cm)	5.1 ± 0.7	5.6 ± 1.5	5.3 ± 0.9	5.5 ± 0.3	ns	ns	ns
N leaves	17.8 ± 3.3	18.6 ± 4.0	17.2 ± 3.4	17.8 ± 2.3	ns	ns	ns
A_L (cm^2)	333.1 ± 70.3	339.9 ± 65.1	218.6 ± 24.8	327.6 ± 38.7	*	*	ns
LMA ($g\ m^{-2}$)	27.3 ± 3.5a	27.2 ± 1.8a	34.9 ± 2.0b	43.0 ± 4.5c	*	***	*
DW plant (mg)	2703.0 ± 231.3	3760.8 ± 456.9	2329.8 ± 813.4	3870.7 ± 743.9	**	ns	ns
DW stem (mg)	343.9 ± 38.0	465.0 ± 120.0	253.6 ± 113.0	424.9 ± 145.1	*	ns	ns
DW leaves (mg)	894.6 ± 166.9a	960.8 ± 159.9a	1022.9 ± 234.4b	1793.9 ± 463.9c	*	**	*
DW bud (mg)	1153.1 ± 186.2	1842.1 ± 453.5	284.5 ± 188.4	726.8 ± 222.3	*	**	ns
DW root (mg)	311.5 ± 41.4	492.3 ± 43.6	768.9 ± 322.5	924.9 ± 227.8	*	**	ns
b) PV-derived	**traits** (n = 5)						
$-\Psi_{tlp}$ (MPa)	1.07 ± 0.04a	1.08 ± 0.06a	1.66 ± 0.12b	1.97 ± 0.1c	**	***	**
$-\pi_o$ (MPa)	0.82 ± 0.07a	0.85 ± 0.06a	1.22 ± 0.09b	1.59 ± 0.08c	***	***	***
ε (MPa)	5.8 ± 1.5a	5.1 ± 1.7a	13.4 ± 2.4b	19.6 ± 4.5c	ns	***	*
RWC_{tlp} (%)	75.2 ± 2.4	74.5 ± 2.9	86.3 ± 4.7	83.4 ± 2.8	ns	***	ns
C^*_{ft} ($mmol\ m^{-2}MPa^{-1}$)	1.92 ± 0.31	1.93 ± 0.45	1.87 ± 0.31	1.73 ± 0.35	ns	ns	ns
C^*_{tlp} ($mmol\ m^{-2}MPa^{-1}$)	4.46 ± 0.66a	8.56 ± 0.99b	4.55 ± 0.94a	4.48 ± 0.70a	***	***	***
SWC ($g\ g^{-1}$)	8.88 ± 1.39	9.14 ± 0.86	9.69 ± 1.13	8.14 ± 2.22	ns	ns	ns
c) WUEi (n = 3)							
Leaf	24.8 ± 16.4	28.9 ± 16.7	74.2 ± 4.4	88.4 ± 21.4	ns	**	ns
Stem	31.6 ± 8.1	55.7 ± 4.9	91.5 ± 14.9	83.8 ± 4.8	ns	**	ns
Root	36.9 ± 2.6	58.6 ± 4.8	94.7 ± 6.8	91.9 ± 11.5	ns	**	ns
d) REL (n = 8)							
REL leaf (%)	13.7 ± 3.5a	14.9 ± 3.6a	26.7 ± 2.9b	17.4 ± 3.9a	**	***	***
REL stem (%)	25.5 ± 5.2	24.7 ± 6.8	23.9 ± 6.6	24.3 ± 3.8	ns	ns	ns
REL root (%)	40.9 ± 6.5a	40.9 ± 5.9a	55.9 ± 7.6b	41.1 ± 10.4a	*	*	*

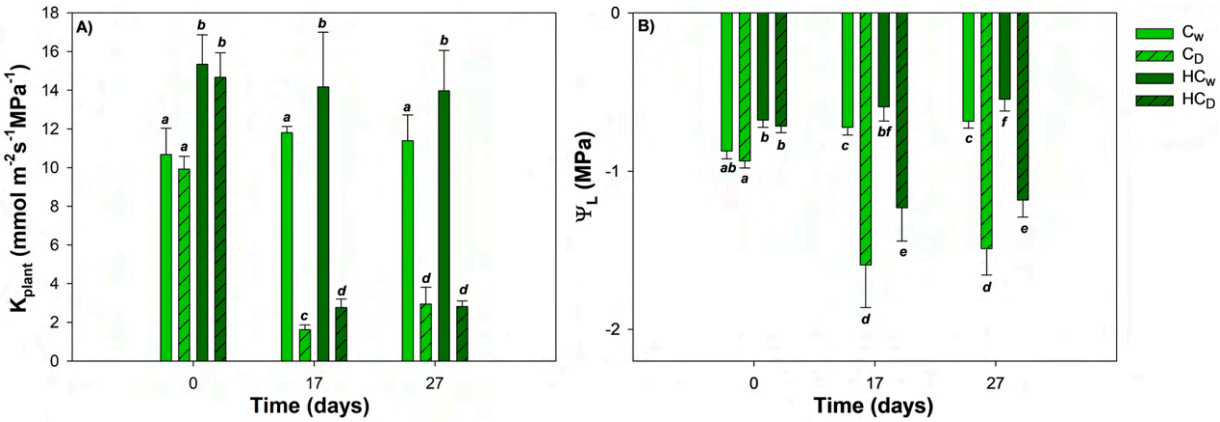

Fig. 2. Mean ± SD values of A) plant hydraulic conductance (K_{plant}) and B) leaf water potential (Ψ_L), measured on the day drought treatment began (day 0), and three days after rewatering following the second (day 17) and third (day 27) drought cycles, in well-watered (C_w and HC_w) and drought-treated (C_D and HC_D) *Helianthus annuus* plants. Different letters indicate statistically significant differences as determined by a two-way ANOVA followed by a Holm-Sidak post-hoc test, accounting for both the growing medium (GM, i.e., substrate, C, and substrate mixed with hydrochar, HC) and the irrigation treatment (I, i.e., regularly watered samples and samples subjected to drought).

function, MF) and KEGG were filtered by Fisher's exact test as well as Bonferroni multi-test adjustment method (Du et al., 2010).

2.11. Weighted gene co-expression network analysis (WGCNA)

Starting from DEGs identified among different treatments, the WGCNA was performed using variance stabilizing transformed (VST) expression data of the gene counts. The correlation between genes was estimated using the Pearson correlation coefficient (PCC), which was used to calculate the distance matrix. WGCNA was performed using the WGCNA R package v. 1.70–3 (Langfelder and Horvath, 2008). The distance matrix was then used for dynamic hierarchical clustering and to build edges (connections) between nodes (genes) in the network. In addition, network topology research was executed from 1 to 40 soft thresholding powers using scale-free topology criteria and used a specific power to identify the co-expressed modules. The minimum module size was set to 30, and the merge cut height was set to 0.15 (to merge modules with at least 85 % similarity). The correlations between one gene and all others were incorporated into an adjacency matrix, which was transformed into a topological matrix (TOM) (Yip and Horvath, 2007). After hierarchical clustering, highly correlated genes were assigned to the same module (Ravasz et al., 2002). Finally, the eigengenes highly associated with specific parameters were considered to select hub genes to construct regulatory networks by using Cytoscape v. 3.10.1 software (Shannon et al., 2003).

2.12. Quantitative real-time PCR verification

Total RNA was isolated from sunflower leaves exposed to drouth stress (C_D) and control (C_w). RNA was extracted using RNeasy Plant Mini Kit (Qiagen, Milano, Italy) according to the manufacturer's protocol and its quality and quantification were assayed using a NanoDrop 2000 (Thermo Scientific). A first-strand cDNA was synthesized from 2 μg of total RNA by using Maxima™ Reverse Transcriptases kit and quantitative expression analysis was performed using the PowerUp™ SYBR™ Green Master Mix (Thermo Fisher) on a QuantStudio® 5 Real-Time PCR System (Applied Biosystems, Europe). The expression profiles of seven hub gene selected were analysed. Finally, the correlation between RNA-seq and qRT-PCR data was determined using a linear model. The gene-specific primers used are listed in Supplementary Table S3.

2.13. Statistical analysis

Statistical analysis was performed using SigmaStat v. 12.0 software (SPSS, Inc., Chicago, IL, USA).

To check differences between growing medium (GM, soil and soil enriched with hydrochar) and the effect of irrigation (I, well-watered versus drought) on Hplant, Ø, number of leaves, LMA, DW, Ψ_{tlp}, π_o, ε, RWC_{tlp}, C^*_{ft}, C^*_{tlp}, SWC (data reported in Table 1a, b), K_{plant} and $-\Psi_L$ (Fig. 2), g_L, E_L, An (Supplementary Figure 9), WUEi and REL in leaf, stem and root (Table 1c, d), two-way ANOVA tests, followed by Pairwise multiple comparisons (Holm-Sidak method) were performed, after verifying normality and homoscedasticity assumptions. To check differences in biomass (Supplementary Figure 8) among growing medium (GM, soil and soil enriched with hydrochar), the effect of irrigation (I, well-watered versus drought) and the organs (O, root, stem, leaf and flower) a three-way ANOVA test, followed by Pairwise multiple comparisons (Holm-Sidak method) was performed, after verifying normality and homoscedasticity assumptions.

3. Results

3.1. Physical-chemical characterization of hydrochar

The FT-IR spectrum of the hydrochar sample revealed several key features characteristic of biomass-derived carbonaceous materials (Supplementary Figure 2). A broad absorption band centered at 3380 cm^{-1} corresponds to O–H stretching vibrations, indicative of hydroxyl groups. A distinct band at 2390 cm^{-1} suggests the presence of C–H stretching. Peaks at 1700 and 1600 cm^{-1} are attributed to C═O stretching in carboxylic acids or conjugated carbonyl groups and C═C stretching in alkenes, respectively. The absorption at 1430 cm^{-1} is consistent with alkane stretching into methyl groups. Additionally, the peak at 1200 cm^{-1} may arise from either aromatic ring vibrations or C–O stretching in aromatic esters. The band at 1020 cm^{-1} is likely associated with CO–O–CO stretching vibrations.

CHNS-O elemental analysis (Supplementary Figure 3) confirmed the presence of the primary elements in the hydrochar, with a significant abundance of carbon and oxygen. Notably, nitrogen-containing groups were absent, a finding supported by the FT-IR spectrum, which lacked characteristic bands for amine or nitro functionalities (Supplementary Figure 2).

Raman spectroscopy further elucidated the structural features of the hydrochar (Supplementary Figure 4). The spectrum displayed two dominant bands: the D-band at ~1390 cm^{-1} , indicative of structural defects and disorder in graphitic domains, and the G-band at ~1590 cm^{-1} , associated with the in-plane vibration of sp^2-hybridized carbon atoms, characteristic of graphitic structures. A valley observed at

~1480 cm^{-1} is attributed to Kekulé vibrational modes of aromatic rings, suggesting partial aromatic condensation.

UV–Vis spectroscopy revealed a single, intense absorption peak at ~280 nm (Supplementary Figure 5), typical of π–π* transitions in sp^2-conjugated aromatic systems. This also implies the presence of oxygenated functional groups such as carbonyl (C═O) and carboxyl (COOH) moieties, which commonly form during hydrothermal carbonization (HTC).

The morphological characteristics of the hydrochar were examined using SEM (Fig. 1A, B). SEM images showed an amorphous surface interspersed with numerous microspheres, a hallmark of hydrochar derived from lignocellulosic biomass via HTC. These observations confirm the formation of typical HTC-derived structures under the applied conditions.

XRD analysis (Supplementary Figure 6) revealed two weak reflections at $2\theta \approx 15.4^{\circ}$ and 22.8°, corresponding to residual crystalline cellulose. However, the overall diffractogram indicated a predominantly amorphous structure, consistent with extensive depolymerization and condensation during HTC at 240 °C.

TGA conducted under an inert atmosphere (Supplementary Figure 7) demonstrated a major weight loss between 350 °C and 500 °C. This mass loss is attributed to the thermal decomposition of residual biodegradable organics, such as cellulose, hemicellulose, and their degradation products. These results confirm the partial retention of thermally labile components within the final hydrochar matrix.

3.2. Growing medium properties

Soil mixed with hydrochar exhibited higher water content both at saturation (SWC) and at field capacity (FC) compared to the control soil (SWC: 2.6 vs. 2.1 g g^{-1}; FC: 2.4 vs. 1.7 g g^{-1}, respectively). (Fig. 1C). At soil water potential of −1.5 MPa (i.e., the reference value of permanent wilting point, WP), the water content was 0.7 g g^{-1} for C and 0.97 g g^{-1} for HC. Hence, the amount of water available to plants (AWC), calculated as (SWC-WP), turned out to be approximately 43 % higher in HC (1.4 g g^{-1}) than in C (1.0 g g^{-1}). Moreover, in addition to the higher SWC and AWC values, the dehydration time of soil enriched with hydrochar was longer than that of soil without it (Fig. 1D).

No statistically significant changes in pH, cation exchange capacity (CEC), or electrical conductivity (EC) were recorded among the soil experimental groups (Supplementary Table 1). Similarly, bulk density (approximately 220 kg/m^3) were comparable across the groups. An increase in total carbon and organic carbon, along with a decrease in nitrogen, was observed in the soil amended with hydrochar (Supplementary Table 1).

3.3. Plant growth and morpho-anatomical traits

The presence of hydrochar in the soil and the different irrigation treatments had no impact on the number of leaves or stem diameter (Table 1a). In response to drought, C_D plants showed lower plant height and a reduction in leaf surface area compared to Cw plants. However, this was not the case for HC_D plants, which exhibited a decrease in plant height but no change in leaf surface area compared to well-watered plants. The drought treatment led to an increase in LMA in both C_D and HC_D plants, with HC_D showing the highest LMA values.

Hydrochar led to an approximate 40 % increase in plant biomass (DW plant) in both well-watered and drought-treated plants compared to the control under the same irrigation conditions (i.e., HCw vs. Cw and HC_D vs. C_D, respectively). The productivity of well-watered plants (Cw and HCw) was primarily driven by the production of flowers and leaves, which constituted about 45 % and 30 % of the total plant biomass, respectively (Table 1, Supplementary Figure 8). In drought-treated samples, no decrease in overall plant biomass was observed compared to plants growing in the same growth medium (i.e., Cw vs. C_D and HCw vs. HC_D) (Table 1). Notably, HC_D plants exhibited higher biomass in all organs compared to C_D plants, with bud weight being three times higher than that recorded in C_D plants. Within the same irrigation treatment (watered vs drought) no changes in biomass partitioning occurred.

3.4. Water relations

Drought treatment had a significant impact on PV-derived traits (Table 1b). In response to drought, sunflowers lowered their turgor loss point by reducing osmotic potential (π_o) and increasing cell wall rigidity (ε). Because of the higher cell wall stiffness, irrigation treatment led to an increase in RWC_{tlp} values in C_D and HC_D leaves. In contrast, no changes were measured in SWC values or leaf capacitance at full turgor in the measured leaves.

Isotope analysis revealed a significant increase in WUEi in response to irrigation (Table 1c). Under drought conditions, WUEi increased in all plant organs compared to well-watered conditions. However, no significant differences were observed between control and hydrochar samples.

The presence of hydrochar in the soil improved plant performance, particularly during the first weeks of growth (Supplementary Figure 9). At the start of the drought treatment (referred to as time 0), when the plants were about one month old, the values of g_L, E_L, and An were higher in the hydrochar-treated (HC) samples compared to the control samples. Specifically, g_L was 818.2 ± 41.8 mmol $m^{-2}s^{-1}$ in C vs 1014.8 ± 61.1 mmol $m^{-2}s^{-1}$ in HC ($P < 0.001$), E_L was 9.0 ± 0.6 mmol $m^{-2}s^{-1}$ in vs 10.5 ± 0.4 mmol $m^{-2}s^{-1}$ in HC ($P = 0.001$), An was 9.08 ± 0.7 mmol $m^{-2}s^{-1}$ vs 11.4 ± 0.8 mmol $m^{-2}s^{-1}$ ($P < 0.001$). This trend persisted during the first week of drought treatment. Correspondingly, during the first 7 days of treatment (0−7), stomatal conductance to water vapor was approximately 950 mmol m^2s^{-1} in both HCw and HC_D, while it did not exceed 750 mmol m^2s^{-1} in Cw and C_D. Similarly, in the same period, An was about 9.5 mmol m^2s^{-1} in HCw but did not exceed 8.5 mmol m^2s^{-1} in Cw and was about 8 mmol m^2s^{-1} in HC_D but no more than 5 mmol m^2s^{-1} in C_D. As expected, the drought treatment resulted in a significant reduction in gas exchange. Consequently, C_D and HC_D showed similar values for the measured parameters during days 8–14 and 15–27.

The efficiency of long-distance water transport (K_{plant}) was higher in hydrochar-treated samples compared to the control at the start of the drought treatment (approximately 15 vs. 11 mmol m^2s^{-1} MPa^{-1}) (Fig. 2A, Supplementary Table 2).

In response to the drought-re-irrigation cycle, specifically three days after the first re-irrigation (day 17), C_D and HC_D exhibited a notable reduction in K_{plant} compared to Cw and HCw. Additionally, it is worth noting that the hydraulic conductance of HC_D plants was higher than that measured in C_D samples. At the end of the experimental period, three days after the second re-irrigation, Cw and HCw continued to maintain the same values recorded at time 0 (i.e., 11 and 15 mmol m^2s^{-1} MPa^{-1}), while C_D and HC_D showed similar values of approximately 3 mmol m^2s^{-1} MPa^{-1} .

C_D leaves demonstrated a lower ability to recover water status after drought events compared to HC_D leaves (Fig. 2B). Specifically, the water potential values were more negative in C_D samples than in HC_D samples. Additionally, despite similar relative electrolyte leakage (REL) values recorded in the cell stems of all experimental groups, the root and leaf cells of C_D plants exhibited greater damage from drought events (Table 1c).

3.5. Transcriptomic sequencing

In order to identify the molecular mechanisms underlying the effects of hydrochar on drought tolerance, we performed transcriptomic sequencing of the leaf in plants exposed to Cw, C_D, HCw and HC_D. After adapter trimming and removal of low-quality reads, the Q30 values ranged from 95.5 % to 98.8 %, and the GC content varied between 47 % and 48 %. Moreover, 81.18–86.65 % of the clean reads were uniquely

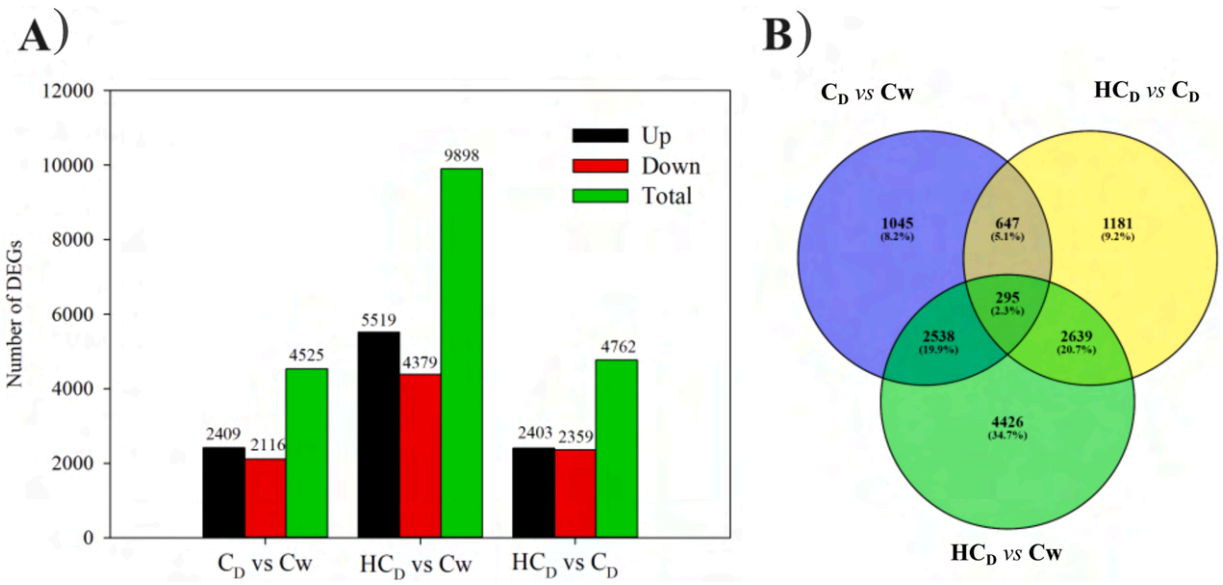

Fig. 3. A) Number of DEGs in different treatments; B) Venn diagram analysis to show the overlap or specific DEGs among different treatments.

mapped to the *Helianthus annuus* reference genome (Supplementary Table 4).

Principal component analysis (PCA) of transcriptomic profiles showed a high degree of clustering among the three biological replicates. While samples from HCw and Cw exhibited similar expression patterns, distinct transcriptional responses were observed in C and HC under drought conditions (Supplementary Figure 10).

Differential gene expression analysis using DESeq2, with thresholds set at $\log_2$(fold change) $> |1|$ and adjusted p-value < 0.05, identified 4525 DEGs (2409 upregulated and 2116 downregulated) in C_D vs Cw, 9898 DEGs (5519 upregulated and 4379 downregulated) in HC_D vs Cw, and 4762 DEGs (2403 upregulated and 2359 downregulated) in HC_D vs C_D (Fig. 3A).

Although the number of DEGs in C_D vs Cw and HC_D vs C_D was comparable, their expression profiles differed qualitatively. A total of 269 DEGs were shared among all three comparisons, whereas 1045, 1181, and 4426 DEGs were uniquely expressed in C_D vs Cw, HC_D vs C_D, and HC_D vs Cw, respectively (Fig. 3B).

Additionally, 452 transcription factors (TFs) were identified among the 12,771 DEGs, highlighting the potential regulatory mechanisms involved in the response to drought and hydrochar treatment.

3.6. Functional annotation analysis of DEGs

Gene Ontology (GO) enrichment analysis revealed both distinct yet overlapping functional responses across treatments (C_D vs Cw, HC_D vs C_D, and HC_D vs Cw), highlighting both drought- and hydrochar-induced molecular adjustments (Fig. 4).

In the C_D vs Cw enriched biological processes were mainly related to photosynthesis, chloroplast organization, and light harvesting, together with genes involved in detoxification and transmembrane transport, indicating a coordinated regulation of energy metabolism and stress adaptation (Fig. 4).

In HC_D vs C_D, enrichment of carbon metabolism, ribosome biogenesis, and response to light stimulus suggested enhanced photosynthetic activity and protein synthesis under hydrochar amendment (Fig. 4). The HC_D vs Cw comparison exhibited the broadest enrichment across categories, involving photosynthesis, chlorophyll and isoprenoid biosynthesis, protein phosphorylation, and vesicle-mediated transport, reflecting a comprehensive metabolic and signalling reprogramming under combined hydrochar and drought stress (Fig. 4).

Consistently, cellular component terms were dominated by chloroplast- and thylakoid-associated genes, while molecular functions included oxidoreductase, transporter, and transcription factor activities, indicating an integrated redox and regulatory adjustment to stress conditions

KEGG pathway enrichment further supported these findings (Fig. 5). Across all comparisons, major pathways involved carbon and amino acid metabolism, photosynthesis, and biosynthesis of secondary metabolites, reflecting a global reorganization of primary and secondary metabolism. In particular, HC_D treatments enhanced carbon fixation, fatty acid biosynthesis, and chlorophyll metabolism, suggesting improved photosynthetic performance and membrane remodelling. These results collectively point to hydrochar-mediated reinforcement of energy metabolism and stress-defence pathways under drought conditions.

3.7. Gene Co-expression modules and their associations with physiological traits

To elucidate the functional relevance of co-expressed gene modules in relation to key physiological traits, we performed a Weighted Gene Co-expression Network Analysis (WGCNA).

From the 12.771 differentially expressed genes (DEGs) across treatments, 17 merged co-expression modules were constructed (Supplementary Figure 11a). Module sizes varied considerably, ranging from 3.562 genes in the *black* module to only 69 genes in the *ivory* and *lightcyan1* modules (Supplementary Figure 11B). Correlation analysis between module eigengenes and physiological traits (REL leaf, Ψ_{tlp}, πo, E_L, An, WUEi) identified several modules strongly associated with drought-related response ($|r| > 0.8$, $p < 0.05$; Fig. 6).

The black, darkmagenta, and orange modules showed the strongest correlations with water-use efficiency and drought-related parameters, representing key targets for functional exploration. The black module was positively correlated with WUEi ($r = 0.81$), Ψ_{tlp} ($r = 0.64$), and πo ($r = 0.70$), indicating a potential role in water-use efficiency and drought resistance. The darkmagenta module was positively associated with REL_{leaf} ($r = 0.85$) and An ($r = 0.57$), suggesting involvement in membrane stability and photosynthetic maintenance. The orange module was also correlated with WUEi ($r = 0.86$), reinforcing its potential role in water-use regulation.

Network analysis of the *darkmagenta* module (128 nodes, 299 edges) identified several hub genes (Fig. 7), including LOC110878709 (*dehydrodolichyl diphosphate synthase 6*), LOC110879135 (*protein LHY*), LOC110879133 (*putative circadian clock associated 1*), LOC110879509

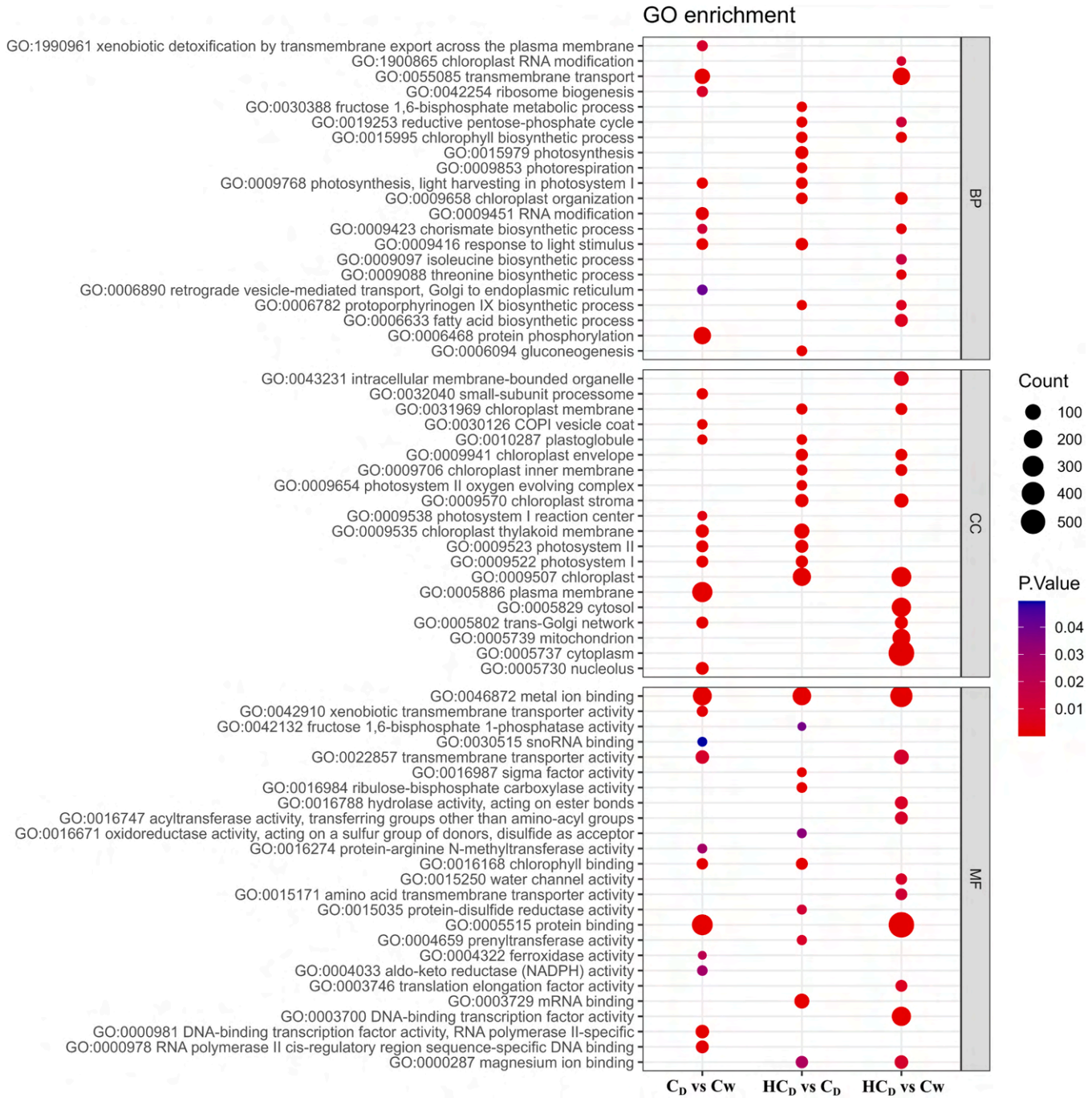

Fig. 4. Gene Ontology (GO) enrichment analysis of differentially expressed genes in sunflower under various treatment comparisons. The bubble plot displays enriched GO terms categorized into Biological Process (BP), Cellular Component (CC), and Molecular Function (MF) for the comparisons C_D vs Cw, HC_D vs C_D, and HC_D vs Cw. The size of each bubble indicates the number of genes associated with a given GO term (Count), while the colour gradient represents the significance level (adjusted p-value).

(*deSI-like protein At4g17486*), LOC110917079 (*acyl-CoA–sterol O-acyltransferase 1*), LOC110865391 (*delta-1-pyrroline-5-carboxylate synthase*). In the orange module (45 nodes, 111 edges), hub genes included LOC110873217 (*shaggy-related protein kinase delta*), LOC110879889 (*cyclin-dependent kinase G-2*), LOC110901511, LOC110911187 (*uncharacterized proteins*), LOC110920491 (*F-box/FBD/LRR-repeat-containing protein*), LOC110937058 (*protein DEHYDRATION-INDUCED 19 homolog 4*). Within the black module, hub genes with putative roles in stress and metabolic regulation included LOC110865063 (*ethylene-responsive transcription factor RAP2–3*), LOC110879425 (*trimethylguanosine synthase*), LOC110866574 (*EARLY RESPONSIVE TO DEHYDRATION 15*), LOC110894858 (*monooxygenase 1*), LOC110887595 (*stress-response A/B barrel domain-containing protein DABB1-like*), LOC110874237 (*alcohol dehydrogenase 2*), LOC110897976 (*zinc finger CCCH domain-containing protein 11-like*).

To further explore the molecular response of sunflower plants to drought stress and hydrochar treatment, we analyzed the expression patterns of key hub genes identified through Weighted Gene Co-expression Network Analysis (WGCNA). Nineteen hub genes were grouped into three co-expression modules, black, orange, and darkmagenta, each of which demonstrated distinct transcriptional responses to the treatments. Genes in the black module (e.g., RAP2.3 transcription

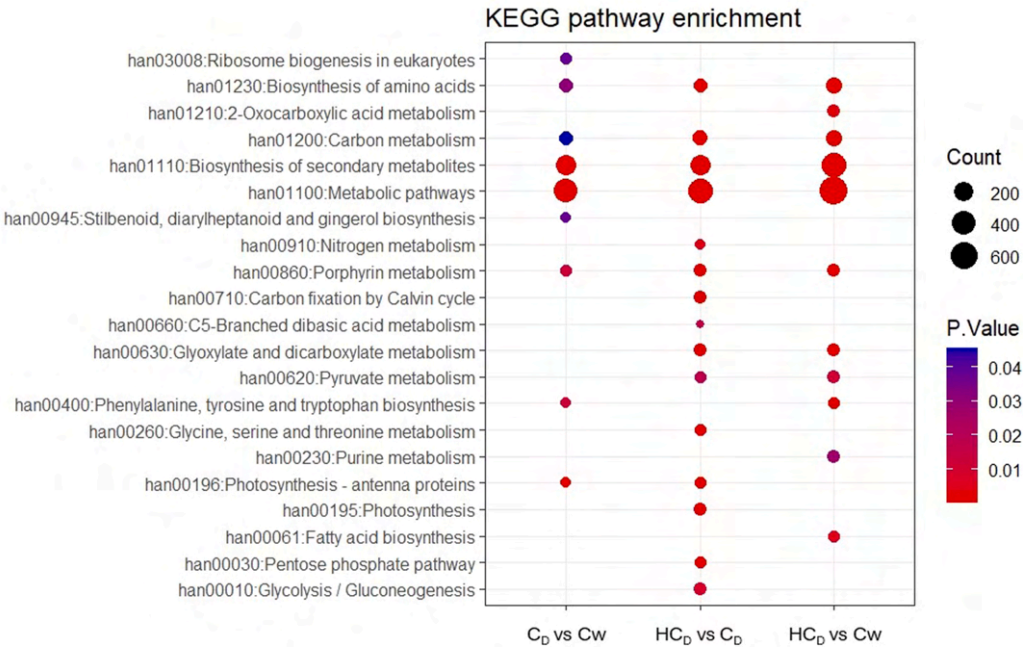

Fig. 5. KEGG pathway analysis of differentially expressed genes in sunflower under various treatment comparisons (C_D vs Cw, HC_D vs C_D, and HC_D vs Cw). The size of each bubble indicates the number of genes associated with a given pathway (Count), while the colour gradient represents the significance level (adjusted p-value), with red indicating higher significance.

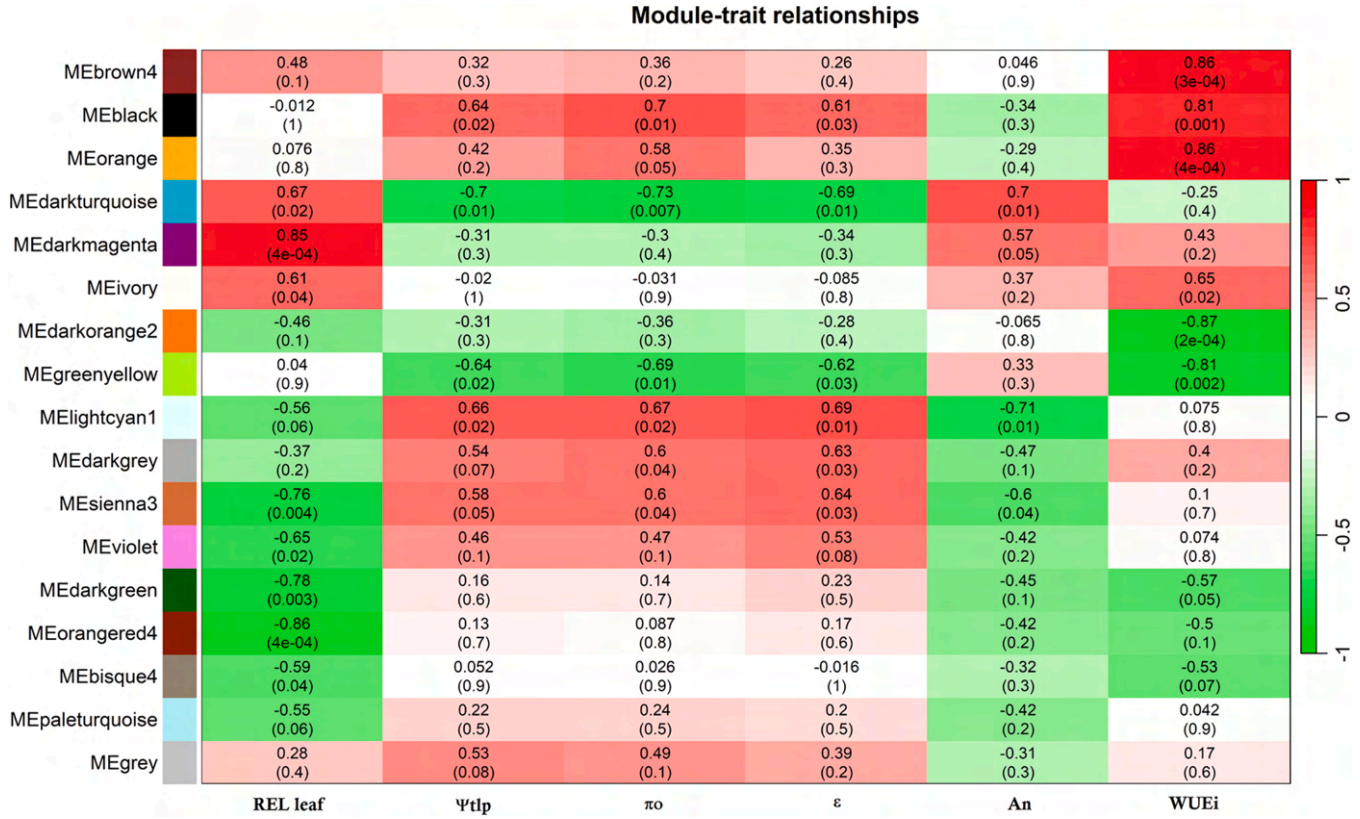

Fig. 6. Correlations of physiological indicators with WGCNA modules. Each row corresponds to a module, while the columns correspond to physiological indicators. The colour of each cell indicates the correlation coefficient between the module and physiological indicator (the top number in the cell represents the correlation coefficient, and bottom one in parentheses represents the P value). REL leaf, relative electrolyte leakage of the leaf; Ψ_{tlp}, leaf water potential at the turgor loss point; π_0, osmotic potential at full turgor; ε, bulk modulus of elasticity; An, photosynthesis rate; WUEi, intrinsic water use efficiency.

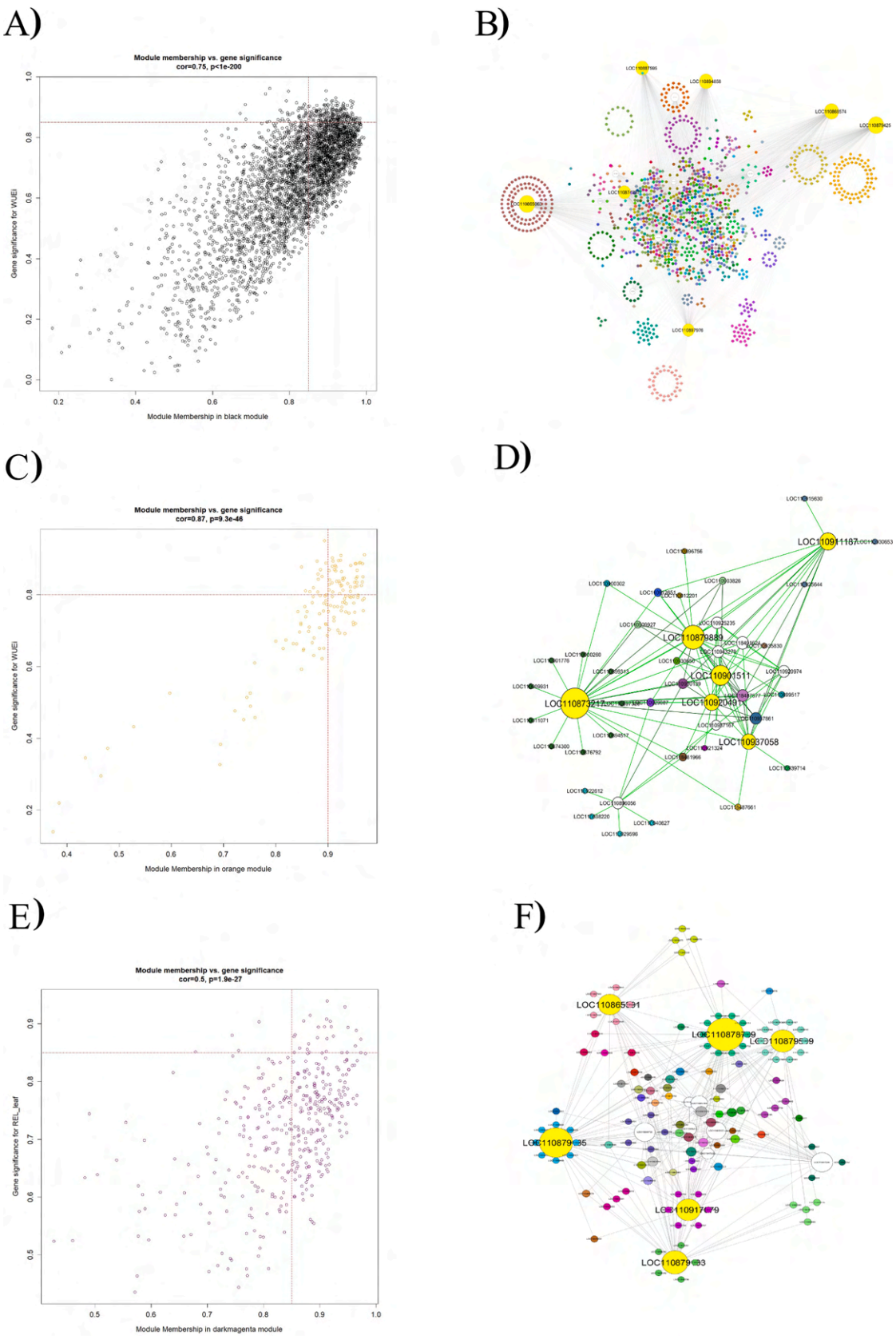

Fig. 7. Tight correlation between gene significance (GS) and module membership (MM) in the three WGCNA modules that best correlate with morpho-physiological traits (black (A), orange (C), and dark magenta (E) modules). The correlation networks of hub genes in each module (black (B), orange (D), and dark magenta (F) modules). Hub genes identified by the highest weights in the weighted gene co-expression network analysis (WGCNA) within each network are highlighted in yellow and labelled based on their annotations.

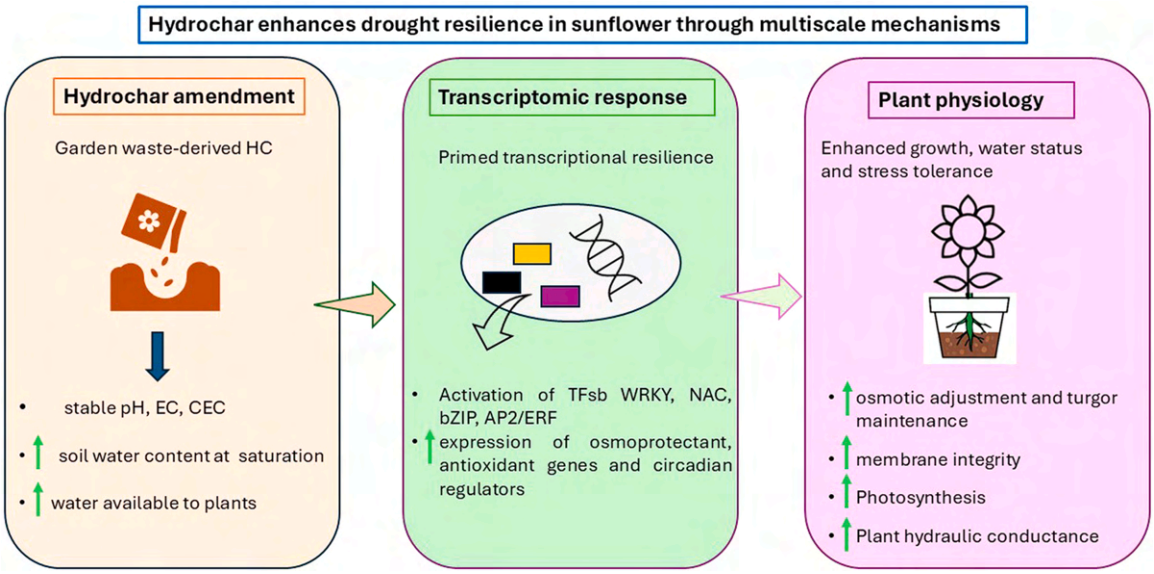

Fig. 8. Hydrochar derived from garden waste significantly enhances drought tolerance in *Helianthus annuus* L. by improving soil water retention, which in turn modulates key stress-responsive gene networks involved in plant hydraulics and overall drought resilience.

factor, trimethylguanosine synthase, EARLY RESPONSIVE TO DEHYDRATION 15) showed strong upregulation under both drought (C_D) and hydrochar + drought (HC_D) conditions compared to the control (Supplementary Figure 13), whereas the EARLY RESPONSIVE TO DEHYDRATION 15 gene exhibited peak expression under drought stress alone, with slightly reduced expression in the HC_D treatment,.

Finally, within the black module, 12 transcription factors were specifically induced by hydrochar under drought (HCD vs. CD), including WRKY, NAC, bZIP, AP2/ERF, and GATA family members (Supplementary Fig. 14; Supplementary Table 5). Although some of these transcription factors have not been experimentally validated for drought response, their co-expression and module-trait correlations indicate a potential regulatory role in stress adaptation.

4. Discussion

This study demonstrates how hydrochar, derived from garden waste, can enhance drought resilience in sunflower by modulating soil water dynamics, improving plant physiological performance, and reprogramming stress-related gene networks (Fig. 8). By integrating soil, physiological, and transcriptomic data, we provide a comprehensive picture of HC's role as a multifunctional soil amendment.

4.1. Hydrochar improves soil water retention while preserving chemical balance

The garden waste-derived hydrochar used in this study displayed distinctive physicochemical properties (high carbon content, structural disorder, abundant oxygenated functional groups, and thermal stability) that underpin its water-retentive capacity. HC significantly increased soil water retention, raising available gravimetric water content at the standard permanent wilting point of −1.5 MPa by ~43 % compared to controls. This result aligns with findings in coarse-textured soils (Liu et al., 2018; de Jesus et al., 2019) and is likely attributable to HC's porous architecture and abundance of hydrophilic functional groups (e.g., carboxyl, hydroxyl, phenolic moieties), which promote water sorption and reduce evaporation.

Extended dehydration times observed in HC-treated soils further support this mechanism, in line with earlier observations (Kamb and Dutta, 2015; Kravchenko et al., 2024). Moreover, HC's aromatic domains and disordered carbon matrix may facilitate the adsorption of organic and inorganic pollutants, suggesting additional value in environmental remediation (Khan et al., 2020).

Crucially, HC application did not significantly affect key soil chemical parameters (pH, cation exchange capacity, electrical conductivity, bulk density), confirming that water retention improvements occur without altering the chemical balance of the soil. This finding corroborates studies using similarly processed garden waste-derived HC (Suárez et al., 2023), though deviations have been reported with alternative feedstocks or HTC conditions (de Jager and Gianim, 2021), underlining the importance of source material and processing parameters (Kalderis. et al., 2019; Zhao et al., 2024).

While HC increased both total and organic carbon in soils, an expected effect of its carbon-rich composition, nitrogen levels declined, possibly due to altered nitrogen speciation or volatilization during hydrothermal processing (Kruse et al., 2016; Alhnidi et al., 2020; Xie et al., 2023). Given its lignocellulosic structure and high availability, garden waste emerges as a viable and sustainable feedstock for HC production (Fregolente et al., 2021).

In summary, garden waste-derived HC offers an effective strategy to improve soil water retention without disrupting chemical equilibrium, while potentially contributing to long-term carbon sequestration and circular economy strategies in agriculture.

4.2. Hydrochar promotes growth and water use under both optimal and drought conditions

HC-treated *H. annuus* plants showed enhanced performance under both irrigation regimes. While literature reports diverging plant responses to HC, ranging from growth promotion (de Jager and Gianim, 2021; Battipaglia et al., 2023) to inhibition (Luutu et al., 2022), such variability likely reflects differences in feedstock composition, HTC parameters, and experimental setups.

Here, we integrated morphological, physiological, and hydraulic data to elucidate HC's role beyond biomass outcomes. Under well-watered conditions, HC improved total biomass across vegetative and reproductive organs, paralleled by enhanced photosynthesis, increased gas exchange efficiency, and higher whole-plant hydraulic conductance. These outcomes are consistent with improved root-stem-leaf hydraulic architecture and greater carbon gain (Raimondo et al., 2009; Rodríguez Gamir et al., 2016; Creek et al., 2018).

Drought stress revealed even more pronounced HC effects. Biomass

production in HC-treated droughted plants (HC_D) was comparable to well-watered controls, suggesting that enhanced pre-stress growth and carbon reserves buffered drought-induced declines. Notably, biomass allocation shifted toward roots and leaves, indicated by higher LMA and reduced investment in buds, reflecting a strategy favoring water uptake and stress tolerance. Still, bud biomass in HC_D remained substantially higher than in C_D plants, suggesting that HC also helps sustain reproductive development under stress.

Although total biomass was maintained under drought in both control and hydrochar-treated plants, it is reasonable to hypothesize that the reduced photosynthetic rate may have limited the accumulation of non-structural carbohydrates (NSCs), which serve as carbon reserves and precursors for secondary metabolites. This hypothesis warrants testing in future studies.

Physiological analyses confirmed drought tolerance mechanisms. HC-treated plants showed more negative turgor loss point and osmotic potential, greater cell wall rigidity, and higher LMA, classic indicators of osmotic adjustment and dehydration tolerance (Bartlett et al., 2012; Zhou et al., 2018; Nardini, 2022).

Moreover, membrane integrity was better preserved in HC_D plants, with relative electrolyte leakage similar to that of unstressed plants. Membrane stabilization is essential for maintaining cellular homeostasis under drought (Guadagno et al., 2017; Trifilò et al., 2021), and its preservation likely contributes to HC-mediated stress mitigation at the cellular level.

In conclusion, HC improves plant growth and physiological performance under favorable conditions while significantly enhancing tolerance to water deficit. These benefits arise from coordinated effects on water relations, hydraulic conductance, and membrane stability, supporting HC's value in sustainable cropping systems facing increasing drought risks. The effects of HC on plant performance may arise from direct actions of bioactive compounds or indirect benefits through improved soil properties and water availability. While we did not measure microbial and chemical contributions in this study, the observed improvements in plant performance suggest that both mechanisms may contribute. Future work should aim to disentangle these effects by assessing HC bioactive compounds and soil-microbe interactions, providing a more complete understanding of the pathways through which HC enhances drought resilience.

4.3. *Hydrochar reprograms drought-responsive transcriptional networks*

Transcriptomic data revealed that HC modulates drought responses at the molecular level, especially under stress. While transcriptomes of well-watered HC and control plants were largely similar, HC-treated plants under drought exhibited a distinct transcriptional profile compared to untreated droughted plants, suggesting an active priming or reprogramming effect rather than passive amplification (Wu et al., 2022).

A key feature was the differential expression of 452 transcription factors (TFs), many uniquely upregulated in HCD plants. These included members of WRKY, NAC, bZIP, bHLH, TCP, and AP2/ERF families, known to regulate hormonal signaling, osmoprotection, and redox homeostasis (Manavella et al., 2006; Singh and Laxmi, 2015; Wang et al., 2022; Li et al., 2022; Zhou et al., 2024).

GO enrichment analysis of DEGs in C_D plants highlighted chloroplast-related pathway, photosynthesis, plastid organization, chlorophyll biosynthesis, reflecting stress impacts on plastid function (Zahra et al., 2023; Zaib et al., 2023). Enriched terms in HC_D plants also included xenobiotic detoxification and membrane transport pathways, suggesting HC primes protective and detoxifying responses to mitigate oxidative and osmotic damage.

WGCNA identified gene co-expression modules tightly linked to physiological traits. The black module, positively correlated with WUEi, πo, and Ψtlp, contained hub genes such as *monooxygenase 1 (LOC110894858)*, *RAP2.3*, and *ERD15*. These genes are involved in secondary metabolism, ethylene signaling, and early dehydration responses, and were strongly upregulated under drought but partially or fully restored in HC_D plants, indicative of HC's capacity to reinforce and stabilize key drought regulatory circuits (Moschen et al., 2017; Shen et al., 2023; Moroldo et al., 2024).

The darkmagenta module, linked to net photosynthesis and membrane stability, comprised circadian regulators (*LHY*, *putative CCA1*) and lipid metabolism genes, suggesting time-of-day coordination of stress responses and membrane remodelling (Marcolino Gomes et al., 2014; Yi et al., 2022; Moroldo et al., 2024).

A third co-expression cluster, the orange module, was enriched in genes related to protein phosphorylation, signal transduction, and general stress responses. Hub genes such as *protein kinase* (LOC110873217) were identified as central regulators of phosphorylation-dependent signalling cascades involved in drought adaptation (Moschen et al., 2017). Other important hub genes, such as *trimethylguanosine synthase* and *DABB1-like proteins*, are linked to RNA stabilization and protein folding, further underscoring HC's role in preserving transcriptomic and enzymatic functionality during stress (Giordani et al., 2011; Escalante et al., 2020).

Among the transcription factors upregulated in HC_D-treated plants, several families emerged as potential master regulators of drought tolerance. Members of the WRKY family, such as WRKY51 and WRKY65, are known mediators of ABA-responsive gene networks through their interaction with W-box motifs. In particular, WRKY65 has been recently correlated with enhanced drought tolerance in sunflowers, highlighting its pivotal role in the regulation of stress-responsive pathways (Li et al., 2020), while WRKY51 has been shown to be upregulated under various abiotic stresses, including drought (Gupta et al., 2025; Wang et al., 2026). In addition, NAC transcription factors such as NAC25 and NAC87 were strongly induced by hydrochar treatment. Previous analyses of cis-acting elements and expression profiles of HaNAC genes have indicated that these factors play key roles in osmotic adjustment, antioxidant defense, and cell wall remodeling under salt and drought stress conditions (Li et al., 2021). Collectively, these findings suggest that hydrochar application may enhance drought resilience by modulating a coordinated network of transcriptional regulators involved in ABA signaling and stress adaptation.

Among the transcription factors upregulated in hydrochar-treated sunflower plants under drought, several families emerged as key regulators of developmental plasticity and stress adaptation, including GATA15, RAV1 and TCP15. Although direct functional evidence in *Helianthus annuus* is still limited, homologs of these genes in model species such as *Arabidopsis thaliana* have been implicated in drought-related processes: overexpression of *OsTCP19* imparted drought stress tolerance in Arabidopsis (Mukhopadhyay and Tyagi, 2015). Moreover, a recent study demonstrated that in *Zea mays* ZmTCP42 was involved in drought stress tolerance (Ding et al., 2019).

Similarly, RAV1 (RELATED TO ABI3/VP1) acts as a transcriptional regulator responsive to abscisic acid (ABA) and ethylene; overexpression studies demonstrated that *AtRAV1* and *GhRAV1* modulate drought and salt tolerance by influencing stomatal closure, leaf senescence, and water-use efficiency (Feng et al., 2014; Mittal et al., 2015). Finally, GATA15, though not yet characterized in sunflower, belongs to a TF family known to regulate chlorophyll biosynthesis, carbon metabolism, and stress-induced developmental reprogramming, and in wheat an overexpressed *TaGATA62* and *TaGATA73* in yeast and Arabidopsis enhanced drought and salt tolerance (Du et al., 2023)

Altogether, HC treatment reshaped drought-induced transcriptional dynamics by modulating hormonal signaling pathways, enhancing redox balance and osmotic protection, and preserving membrane and protein stability. These molecular changes tightly mirrored the physiological benefits observed, including improved WUEi, tissue hydration, and stress tolerance traits. Finally, although the present transcriptomic evidence strongly supports the involvement of these transcription factors in the sunflower drought response, further functional studies are

required to elucidate their direct regulatory roles. In particular, targeted experiments such as gene overexpression, loss-of-function analyses, or chromatin immunoprecipitation sequencing (ChIP-seq) will be essential to confirm their downstream targets and to determine whether their induction contributes causally to drought tolerance rather than representing a secondary response to stress.

5. Conclusions

Our integrative study shows that garden waste-derived hydrochar supports drought resilience in *H. annuus* by improving soil water availability, promoting hydraulic and photosynthetic efficiency, and reprogramming gene expression toward enhanced tolerance (Fig. 8). These multifaceted effects underscore the potential of HC as a next-generation bio-based amendment.

Given the variability in HC properties depending on feedstock and HTC conditions, future work should explore genotype × environment × amendment interactions, with a focus on long-term field performance and soil microbiome dynamics. Investigating HC's effects across diverse crops and soil types will be key to scaling its application in climate-smart agriculture.

Ultimately, HC offers a promising strategy to valorize organic waste while improving plant productivity and resilience under water-limited conditions, an urgent goal in the context of global climate change and sustainable food production.

CRediT authorship contribution statement

Patrizia Trifilò: Writing – review & editing, Methodology, Investigation, Funding acquisition, Formal analysis, Data curation, Conceptualization. **Stefano Mileto:** Investigation, Formal analysis, Data curation. **Damiano Spagnuolo:** Investigation, Formal analysis, Data curation. **Antonio Lupini:** Writing – review & editing, Methodology, Investigation, Funding acquisition, Formal analysis, Data curation, Conceptualization. **Giovanna Battipaglia:** Writing – review & editing, Methodology, Investigation, Funding acquisition, Formal analysis, Data curation, Conceptualization. **Viviana Bressi:** Investigation, Formal analysis, Data curation. **Claudia Espro:** Methodology, Investigation, Formal analysis, Data curation. **Giuseppa Genovese:** Writing – review & editing, Methodology, Investigation, Formal analysis, Data curation. **Alessandro Crisafulli:** Investigation, Formal analysis, Data curation. **Domenico Viglianti:** Investigation, Formal analysis, Data curation. **Lucio Zaccariello:** Investigation, Formal analysis, Data curation.

Funding

This study was supported by the European Union – NextGenerationEU- PNRR- Mission 4, Component 2, Investment n.1.1, Call PRIN 2022 PNRR, D.D. 1409 14–09–2022 (Hydrochar application for improving plants performance under stress: a promising pathway to support the transition to a circular economy -HYDRA); CUP: J53D23013850001.

Declaration of Competing Interest

The authors declare that they have no known competing financial interests or personal relationships that could have appeared to influence the work reported in this paper.

Appendix A. Supporting information

Supplementary data associated with this article can be found in the online version at doi:10.1016/j.envexpbot.2025.106281.

Data availability

RNA-seq data is available in the SRA database (BioProject PRJNA1285928) under the link http://www.ncbi.nlm.nih.gov/bioproject/1285928.

References

Alhnidi, M.J., Körner, P., Wüst, D., Pfersich, J., Kruse, A., 2020. Nitrogen-containing hydrochar: the influence of nitrogen-containing compounds on the hydrochar formation. Chem. Open 9 (8), 864–873.

S. Andrews, 2010. FastQC: a quality control tool for high throughput sequence data. http://www.bioinformatics.babraham.ac.uk/projects/fastqc.

Allen, C.D., Breshears, D.D., McDowell, N.G., 2015. On underestimation of global vulnerability to tree mortality and forest die-off from hotter drought in the Anthropocene. Ecosphere 6 (8), 129. https://doi.org/10.1890/ES15-00203.1.

Badouin, H., Gouzy, J., Grassa, C.J., et al., 2017. The sunflower genome provides insights into oil metabolism, flowering and Asterid evolution. Nature 546 (7656), 148–152. https://doi.org/10.1038/nature22380.

Bargmann, I., Rillig, M.C., Kruse, A., Greef, J.-M., Kücke, M., 2014. Effects of hydrochar application on the dynamics of soluble nitrogen in soils and on plant availability. Z. Pflanz. ähr. Bodenk 177, 48–58. https://doi.org/10.1002/jpln.201300069.

Bartlett, M.K., Scoffoni, C., Sack, L., 2012. The determinants of leaf turgor loss point and prediction of drought tolerance of species and biomes: a global meta-analysis. Ecol. Lett. 15, 393–405. https://doi.org/10.1111/j.1461-0248.2012.01751.x.

Battipaglia, G., Niccoli, F., Kabala, J.P., Marzaioli, R., Di Santo, T., Strumia, S., Castaldi, S., Petriccione, M., Zaccariello, L., Battaglia, D., Mastellone, M.L., Coppola, E., Rutigliano, F.A., 2023. Hydrochar application improves growth and intrinsic water use efficiency of Populus alba. Espec. Hot Seas. For. 14 (4), 658. https://doi.org/10.3390/f14040658.

Bento, L.R., Castro, A.J.R., Moreira, A.B., Ferreira, O.P., Bisinoti, M.C., Melo, C.A., 2019. Release of nutrients and organic carbon in different soil types from hydrochar obtained using sugarcane bagasse and vinasse. Geoderma 334, 24–32. https://doi.org/10.1016/j.geoderma.2018.07.034.

Carrasco, S., Pino-Cortés, E., Barra-Marín, A., Fierro-Gallegos, A., León, M., 2022. Use of hydrochar produced by hydrothermal carbonization of lignocellulosic biomass for thermal power plants in Chile: a techno-economic and environmental study. Sustainability 14 (8), 041. https://doi.org/10.3390/su14138041.

Creek, D., Blackman, C.J., Brodribb, T.J., Choat, B., Tissue, D.T., 2018. Coordination between leaf, stem, and root hydraulics and gas exchange in three arid-zone angiosperms during severe drought and recovery. Plant Cell Environ. 41, 2869–2881. https://doi.org/10.1111/pce.13418.

Di Santo, T., Marzaioli, R., Coppola, E., Zaccariello, L., Battaglia, D., Castaldi, S., D'Ascoli, R., Papa, S., Strumia, S., Battipaglia, G., Morra, L., Mastellone, M.L., Rutigliano, F.A., 2025. Enhancing soil health with hydrochar: Improvements in chemical and biological properties. J. Environ. Manag. 385, 125659. https://doi.org/10.1016/j.jenvman.2025.125659.

Ding, S., Cai, Z., Du, H., Wang, H., 2019. Genome-wide analysis of TCP family genes in *Zea mays* L. identified a role for ZmTCP42 in drought tolerance. Int. J. Mol. Sci. 20 (11), 2762 https://www.mdpi.com/1422-0067/20/11/2762.

Dobin, A., Davis, C.A., Schlesinger, F., Drenkow, J., Zaleski, C., Jha, S., Batut, P., Chaisson, M., Gingeras, T.R., 2013. STAR: ultrafast universal RNA-seq aligner. Bioinformatics 29 (1), 15–21. https://doi.org/10.1093/bioinformatics/bts635.

Dong, Y., Yu, B., Jia, Y., Xu, X., Zhou, P., Yu, M., Liu, J., 2025. Influence of sewage sludge compost on heavy metals in abandoned mine land reclamation: a large-scale field study for three years. J. Hazard Mater. 486, 137098. https://doi.org/10.1016/j.jhazmat.2025.137098.

Du, X., Lu, Y., Sun, H., Duan, W., Hu, Y., Yan, Y., 2023. Genome-wide analysis of wheat GATA transcription factor genes reveals their molecular evolutionary characteristics and involvement in salt and drought tolerance. Int. J. Mol. Sci. 24, 27. https://doi.org/10.3390/ijms24010027.

Du, Z., Zhou, X., Ling, Y., Zhang, Z., Su, Z., 2010. agriGO: a GO analysis toolkit for the agricultural community. Nucleic Acids Res. 38, W64–W70.

Escalante, M., Marchand, G., Bazzicalupo, M., Debat, H.J., Carrera, A., Heinz, R.A., 2020. Transcriptomic analysis reveals a differential gene expression profile between two sunflower inbred lines with different ability to tolerate water stress. Plant Cell Rep. 39, 123–137. https://doi.org/10.1007/s11105-020-01192-4.

Farquhar, G., O'Leary, M., Berry, J., 1982. On the relationship between carbon isotope discrimination and the intercellular carbon dioxide concentration in leaves. Austral. J. Plant Physiol. 9, 121–137. doi. https://doi.org/10.1071/PP9820121.

Feng, C.Z., Chen, Y., Wang, C., Kong, Y.H., Wu, W.H., Chen, Y.F., 2014. Arabidopsis RAV1 transcription factor, phosphorylated by SnRK2 kinases, regulates the expression of ABI3, ABI4, and ABI5 during seed germination and early seedling development. Plant J. 80 (4), 654–668. ⟨https://onlinelibrary.wiley.com/doi/full/10.1111/tpj.12670⟩.

Fregolente, L.G., dos Santos, J.V., Mazzati, F.S., et al., 2021. Hydrochar from sugarcane industry by-products: assessment of its potential use as a soil conditioner by germination and growth of maize. Chem. Biol. Technol. Agric. 8, 16. https://doi.org/10.1186/s40538-021-00210-1.

Giordani, T., Natali, L., Margiotta, B., Natali, S., Cavallini, A., Sonnante, G., 2011. An analysis of sequence variability in eight genes putatively involved in drought response in sunflower (Helianthus annuus L.). Theor. Appl. Genet 122, 661–672. https://doi.org/10.1007/s00122-010-1509-0.

Guadagno, C.R., Ewers, B.E., Speckman, H.N., Aston, T.L., Huhn, B.J., DeVore, S.B., Ladwig, J.T., Strawn, R.N., Weinig, C., 2017. Dead or alive? Using membrane failure and chlorophyll a fluorescence to predict plant mortality from drought. Plant Physiol. 175 (1), 223–234. https://doi.org/10.1104/pp.16.00581.

Gupta, D., Regon, P., Mai, H.J., Patel, M., Raje, R.S., Bauer, P., Panda, S.K., 2025. Transcriptional regulation reveals potent drought tolerance mechanisms in contrasting genotypes of Cajanus cajan (L.) Millspaugh. BMC Plant Biol. 25, 1287. https://doi.org/10.1186/s12870-025-07174-6.

Hammond, W.M., Williams, A.P., Abatzoglou, J.T., 2022. Global field observations of tree die-off reveal hotter-drought fingerprint for Earth's forests. Nat. Commun. 13, 1761. https://doi.org/10.1038/s41467-022-29289-2.

Huang, D.W., Sherman, B.T., Lempicki, R.A., 2009. Systematic and integrative analysis of large gene lists using DAVID Bioinformatics Resources. Nat. Protoc. 4, 44–57. https://doi.org/10.1038/nprot.2008.211.

Iizumi, T., Yokozawa, M., Sakurai, G., Travasso, M.I., Romanenkov, V., Oettli, P., Newby, T., Ishigooka, Y., Furuya, J., 2014. Historical changes in global yields. Glob. Ecol. Biogeogr. 23, 346–357. https://doi.org/10.1111/geb.12120.

IPCC, 2022. Climate Change 2022: Impacts, Adaptation and Vulnerability. Contribution of Working Group II to the Sixth Assessment Report of the Intergovernmental Panel on Climate Change. Cambridge University Press, Cambridge, UK & New York, USA. https://doi.org/10.1017/9781009325844.

de Jager, M., Gianim, L., 2021. An investigation of the effects of hydrochar application rate on soil amelioration and plant growth in three diverse soils. Biochar 3, 349–365. https://doi.org/10.1007/s42773-021-00089-z.

de Jesus Duartem, S., Glaserm, B., Pellegrino Cerrim, C.E., 2019. Effect of biochar particle size on physical, hydrological and chemical properties of loamy and sandy tropical soils. Agronomy 9, 165. https://doi.org/10.3390/agronomy9040165.

Kalderis, D., Papameletiou, G., Kayan, B., 2019. Assessment of orange peel hydrochar as a soil amendment: impact on clay soil physical properties and potential phytotoxicity. Waste Biomass. Valor. 10, 3471–3484. https://doi.org/10.1007/s12649-018-0359-0.

Kamb, H.S., Dutta, A., 2015. A comparative review of biochar and hydrochar in terms of production, physico chemical properties and applications. Renew. Sustain Energy Rev. 45, 359–378. https://doi.org/10.1016/j.rser.2015.01.050.

Khan, Z.H., Gao, M., Chen, J., 2020. Adsorption of heavy metals by biochar and hydrochar: A review. Environ. Chem. Lett. 18, 1085–1112. https://doi.org/10.1007/s10311-019-00955-1.

Kompas, T., Che, T.N., Grafton, R.Q., 2024. Global impacts of heat and water stress on food production and severe food insecurity. Sci. Rep. 14, 14398. https://doi.org/10.1038/s41598-024-65274-z.

Kravchenko, E., Dela Cruz, T.L., Sushkova, S., Rajput, V.D., 2024. Effect of wood and peanut shell hydrochars on the desiccation cracking characteristics of clayey soils. Chemosphere 358, 142134. https://doi.org/10.1016/j.chemosphere.2024.142134.

Krueger, F., James, F., Ewels, P., Afyounian, E., Schuster-Boeckler, B. 2021. FelixKrueger/TrimGalore Zenodo https://doi.org/10.5281/zenodo.5127898.

Kruse, A., Koch, F., Stelzl, K., Wüst, D., Zeller, M., 2016. Fate of nitrogen during hydrothermal carbonization. Energy Fuels 30 (10), 8037–8042. https://doi.org/10.1021/acs.energyfuels.6b01312.

Langfelder, P., Horvath, S., 2008. WGCNA: an R package for weighted correlation network analysis. BMC Bioinform. 9, 559. https://doi.org/10.1186/1471-2105-9-559.

Lesk, C., Anderson, W., Rigden, A., et al., 2022. Compound heat and moisture extreme impacts on global crop yields under climate change. Nat. Rev. Earth Environ. 3, 872–889. https://doi.org/10.1038/s43017-022-00368-8.

Li, J., Islam, F., Huang, Q., Wang, J., Zhou, W., Hu, L., Yang, C., 2020. Genome-wide characterization of *WRKY* gene family in *Helianthus annuus* L. and their expression profiles under biotic and abiotic stresses. PLOS ONE 15 (12), e0241965. https://doi.org/10.1371/journal.pone.0241965.

Li, W., Liu, Z., Feng, H., Yang, J., Li, C., 2022. Characterization of the gene expression profile response to drought stress in Populus ussuriensis using PacBio SMRT and Illumina sequencing. Int. J. Mol. Sci. 23, 3840. https://doi.org/10.3390/ijms23073840.

Li, W., Zeng, Y., Yin, F., Wei, R., Mao, X., 2021. Genome-wide identification and comprehensive analysis of the NAC transcription factor family in sunflower during salt and drought stress. Scient. Reports 11, 19865. https://doi.org/10.1038/s41598-021-98107-4.

Liao, Y., Smyth, G.K., Shi, W., 2014. FeatureCounts: an efficient general purpose program for assigning sequence reads to genomic features. Bioinformatics 30 (7), 923–930. https://doi.org/10.1093/bioinformatics/btt656.

Liu, F., Yu, R., Ji, X., Guo, M., 2018. Hydrothermal carbonization of holocellulose into hydrochar: structural, chemical characteristics, and combustion behavior. Bioresour. Technol. 263, 508–516. https://doi.org/10.1016/j.biortech.2018.05.019.

Love, P.E., Warzecha, C., Li, L., 2014. Ldb1 complexes: the new master regulators of erythroid gene transcription. Trends Plant Sci. 30 (1), 1–9.

Luutu, H., Rose, M.T., McIntosh, S., et al., 2022. Plant growth responses to soil-applied hydrothermally-carbonised waste amendments: a meta-analysis. Plant Soil 472, 1–15. https://doi.org/10.1007/s11104-021-05185-4.

Manavella, P.A., Arce, A.L., Dezar, C.A., Bitton, F., Renou, J.-P., Cresp, i M., Chan, R.L., 2006. Cross-talk between ethylene and drought signalling pathways is mediated by the sunflower Hahb-4 transcription factor. Plant J. 48, 125–137. https://doi.org/10.1111/j.1365-313X.2006.02865.x.

Marcolino Gomes, J., Rodrigues, F.A., Fuganti Pagliarini, R., Bendix, C., Nakayama, T.J., Celaya, B., Molinari, H.B.C., Neves de Oliveira, M.C., Harmon, F.G., Nepomuceno, A., 2014. Diurnal oscillations of soybean circadian clock and drought responsive genes. PLoS One 9 (1), e86402. https://doi.org/10.1371/journal.pone.0086402.

Mittal, A., Jiang, Y., Ritchie, G. L., Burke, J. J., Rock, C. D., 2015. AtRAV1 and AtRAV2 overexpression in cotton increases fiber length differentially under drought stress and delays flowering. Plant Sci. 241, 78–95. https://doi.org/10.1016/j.plantsci.2015.09.013.

Molotoks, A., Smith, P., Dawson, T.P., 2021. Impacts of land use, population, and climate change on global food security. Food Energy Secur. 10, e261. https://doi.org/10.1002/fes3.261.

Moroldo, M., Blanchet, N., Duruflé, H., et al., 2024. Genetic control of abiotic stress related specialized metabolites in sunflower. BMC Genom. 25, 199. https://doi.org/10.1186/s12864-024-10104-9.

Moschen, S., Di Rienzo, J.A., Higgins, J., et al., 2017. Integration of transcriptomic and metabolic data reveals hub transcription factors involved in drought stress response in sunflower (Helianthus annuus L.). Plant Mol. Biol. 94, 549–564. https://doi.org/10.1007/s11103-017-0625-5.

Mukhopadhyay, P., Tyagi, A.K., 2015. OsTCP19 influences developmental and abiotic stress signaling by modulatingABI4-mediated pathways. Sci. Rep. 5, 9998. ⟨https://www.nature.com/articles/srep09998⟩.

Nardini, A., 2022. Hard and tough: the coordination between leaf mechanical resistance and drought tolerance. Flora 288, 152023. https://doi.org/10.1016/j.flora.2022.152023.

Nardini, A., Petruzzellis, F., Marusig, D., Tomasella, M., Natale, S., Altobelli, A., Calligaris, C., Floriddia, G., Cucchi, F., Forte, E., Zini, L., 2021. Water 'on the rocks': a summer drink for thirsty trees? N. Phytol. 229, 199–212. https://doi.org/10.1111/nph.16921.

USDA Natural Resources Conservation Service Soil Survey Laboratory Methods Manual (Soil Survey Investigations Report No 2004 U.S. Department of Agriculture Washington, DC.

R Core Team, 2022. R: A language and environment for statistical computing. R Foundation for Statistical Computing, Vienna, Austria. https://www.R-project.org/.

Raimondo, F., Trifilò, P., Lo Gullo, M.A., Andri, S., Savi, T., Nardini, A., 2015. Plant performance on Mediterranean green roofs: interaction of species specific hydraulic strategies and substrate water relations. AoB Plants 7, plv007. https://doi.org/10.1093/aobpla/plv007.

Raimondo, F., Trifilò, P., Lo Gullo, M.A., Buffa, R., Nardini, A., Salleo, S., 2009. Effects of reduced irradiance on hydraulic architecture and water relations of two olive clones with different growth potentials. Environ. Exp. Bot. 66, 249–256. https://doi.org/10.1016/j.envexpbot.2009.03.022.

Ravasz, E., Somera, A.L., Mongru, D.A., Oltvai, Z.N., Barabási, A.L., 2002. Hierarchical organization of modularity in metabolic networks. Science 297 (5586), 1551–1555. https://doi.org/10.1126/science.1073374.

Reza, M.T., Andert, J., Wirth, B., Busch, D., Pielert, J., Lynam, J.G., Mumme, J., 2014. Hydrothermal carbonization of biomass for energy and crop production. Appl. Bioenergy 1 (1), 11–29. https://doi.org/10.2478/apbi-2014-0001.

Rodríguez Gamir, J., Primo Millo, E., Forner Giner, M.Á., 2016. An integrated view of whole tree hydraulic architecture: Does stomatal or hydraulic conductance determine whole tree transpiration? Plos One 11 (5), e0155246. https://doi.org/10.1371/journal.pone.0155246.

Shannon, P., Markiel, A., Ozier, O., Baliga, N.S., Wang, J.T., Ramage, D., Amin, N., Schwikowski, B., Ideker, T., 2003. Cytoscape: a software environment for integrated models of biomolecular interaction networks. Genome Res 13 (11), 2498–2504. https://doi.org/10.1101/gr.1239303.

Shen, J., Wang, X., Song, H., Wang, M., Niu, T., Lei, H., Qin, C., Liu, A., 2023. Physiology and transcriptomics highlight the underlying mechanism of sunflower responses to drought stress and rehydration. iScience 26 (11), 108112. https://doi.org/10.1016/j.isci.2023.108112.

Sherman, B.T., Hao, M., Qiu, J., Jiao, X., Baseler, M.W., Lane, H.C., Imamichi, T., Chang, W., 2022. DAVID: a web server for functional enrichment analysis and functional annotation of gene lists. Nucleic Acids Res. 50 (W1), W216–W221. https://doi.org/10.1093/nar/gkac194.

Singh, D., Laxmi, A., 2015. Transcriptional regulation of drought response: a tortuous network of transcriptional factors. Front. Plant Sci. 6, 895. https://doi.org/10.3389/fpls.2015.00895.

Sleutel, S., De Neve, S., Singier, B., Hofman, G., 2007. Quantification of organic carbon in soils: a comparison of methodologies and assessment of the carbon content of organic matter. Commu. Soil Sci. Plant Anal. 38 (19–20), 2647–2657. https://doi.org/10.1080/00103620701662877.

Springer, U., Klee, J., 1954. Prüfung der Leistungsfähigkeit von einigen wichtigeren Verfahren zur Bestimmung des Kohlenstoffs mittels Chromschwefelsäure sowie Vorschlag einer neuen Schnellmethode. Z. F. üR. Pflanz. ährung D. üngung und Bodenkd. 64, 1–26. https://doi.org/10.1002/jpln.19540640102.

Suarez, E., Martinez-Sanchez, L., de la Rubia, M.A., Reguera, M., Esteban, E., Mohedano, A.F., Tobajas, M., 2025. Assessment of food waste hydrochar as a soil amendment: effects on soil properties, plant growth and stress response. Waste Manag. 204, 114901. https://doi.org/10.1016/j.wasman.2025.114901.

Suarez, E., Tobajas, M., Mohedano, A.F., et al., 2023. Effect of garden and park waste hydrochar and biochar in soil application: a comparative study. Biomass. Conv. Bioref. 13, 16479–16493. https://doi.org/10.1007/s13399-023-04015-0.

Taskin, E., de Castro Bueno, C., Allegretta, I., Terzano, R., Rosa, A.H., Loffredo, E., 2019. Multianalytical characterization of biochar and hydrochar produced from waste biomasses for environmental and agricultural applications. Chemosphere 233, 422–430. https://doi.org/10.1016/j.chemosphere.2019.05.204.

Trifilò, P., Abate, E., Petruzzellis, F., Azzarà, M., Nardini, A., 2023. Critical water contents at leaf, stem and root level leading to irreversible drought-induced damage in two woody and one herbaceous species. Plant Cell Environ. 46, 119–132. https://doi.org/10.1111/pce.14469.

Trifilò, P., Petruzzellis, F., Abate, E., Nardini, A., 2021. The extra-vascular water pathway regulates dynamic leaf hydraulic decline and recovery in *Populus nigra*. Physiol. Plant 172, 29–40. https://doi.org/10.1111/ppl.13266.

Tyree, M.T., Hammel, H.T., 1972. The measurement of the turgor pressure and the water relations of plants by the pressure-bomb technique. J. Exp. Bot. 23 (1), 267–282. https://doi.org/10.1093/jxb/23.1.267.

Wang, H., Li, H., Wang, J., Song, J., Sui, N., 2026. The WRKY transcription factor SbWRKY51 positively regulates salt tolerance of Sorghum. Plant Science 362, 112741. https://doi.org/10.1016/j.plantsci.2025.112741.

Wang, Y., Wu, X., Li, H., Hao, M., Zhang, R., 2022. Transcriptomic and physiological responses of contrasting maize genotypes to drought stress. Front. Plant Sci. 13, 928897. https://doi.org/10.3389/fpls.2022.928897.

Wu, Y., Wang, Y., Shi, H., Hu, H., Yi, L., Hou, J., 2022. Time-course transcriptome and WGCNA analysis revealed the drought response mechanism of two sunflower inbred lines. PLoS One 17 (4), e0265447. https://doi.org/10.1371/journal.pone.0265447.

Xie, L., Gou, L., Xu, D., Kapusta, K., Dai, L., Wang, Y., 2023. Coupling influences of organic components and temperature on nitrogen transformation and hydrochar characterization during hydrothermal carbonization of sewage sludge. Sci. Total Environ. 866, 161354. https://doi.org/10.1016/j.scitotenv.2022.161354.

Yan, T., Zhang, Z., Zhang, Z., Wang, W., Li, D., Zhang, T., Zhu, Z., 2024. Applying hydrochar affects soil carbon dynamics by altering the characteristics of soil aggregates and microbes. Agronomy 14, 1015. https://doi.org/10.3390/agronomy14051015.

Yi, S., Lu, H., Tian, C., Xu, T., Song, C., Wang, W., Wei, P., Gu, F., Liu, D., Cai, Y., et al., 2022. Selection of suitable reference genes for gene expression normalization studies in *Dendrobium huoshanense*. Genes 13, 1486. https://doi.org/10.3390/genes13081486.

Yip, A.M., Horvath, S., 2007. Gene network interconnectedness and the generalized topological overlap measure. BMC Bioinform. 8, 22. https://doi.org/10.1186/1471-2105-8-22.

Zahra, N., Hafeez, M.B., Kausar, A., Al Zeidi, M., Asekova, S., Siddique, K.H.M., Farooq, M., 2023. Plant photosynthetic responses under drought stress: Effects and management. J. Agron. Crop Sci. 209, 651–672. https://doi.org/10.1111/jac.12652.

Zaib, P., Ahmad, H.M., Attacha, S., Rahman, M.-U., Shafiq, M.R., Parveen, K., Fiaz, S., Attia, K.A., Ishaq, S., Arif, S., Abushady, A.M., Umer, M.J., 2023. Comparative genomics of light harvesting chlorophyll (LHC) gene family and impact of chlorophyll-a contents under drought stress in *Helianthus annuus*. J. Plant Physiol. 291, 154136. https://doi.org/10.1016/j.jplph.2023.154136.

Zhao, S., Liu, G., Xiong, J., et al., 2024. Evaluation of hydrochar-derived modifier and water-soluble fertilizer on saline soil improvement and pasture growth. Sci. Rep. 14, 16759. https://doi.org/10.1038/s41598-024-66615-8.

Zhou, Y.B., Liu, C., Tang, D.Y., Yan, L., Wang, D., Yang, Y.-Z., Gui, J.S., Zhao, X.-Y., Li, L. G., Tang, X.D., Yu, F., Li, J.L., Liu, L.L., Zhu, Y.H., Lin, J.Z., Liu, X.M., 2018. The receptor-like cytoplasmic kinase STRK1 phosphorylates and activates CatC, thereby regulating H_2O_2 homeostasis and improving salt tolerance in rice. Plant Cell 30 (5), 1100–1118. https://doi.org/10.1105/tpc.17.01000.

Zhou, Y.B., Wang, Y., Zhang, D., Liang, J., 2024. Endomembrane biased dimerization of ABCG16 and ABCG25 transporters determines their substrate selectivity in ABA regulated plant growth and stress responses. Mol. Plant 17 (3), 478–495. https://doi.org/10.1016/j.molp.2024.02.005.

Zhu, P., Burney, J., Chang, J., et al., 2022. Warming reduces global agricultural production by decreasing cropping frequency and yields. Nat. Clim. Change 12, 1016–1023. https://doi.org/10.1038/s41558-022-01492-5.